






## Activities of $^{223}\text{Ra}$ and $^{226}\text{Ra}$ in Fluids From the Lost City Hydrothermal Field Require Short Fluid Residence Times

 W. S. Moore<sup>1</sup> , J. D. Frankle<sup>1,2</sup> , C. R. Benitez-Nelson<sup>1</sup> , G. L. Früh-Green<sup>3</sup> , and S. Q. Lang<sup>1</sup> 
<sup>1</sup>School of the Earth, Ocean, and Environment, University of South Carolina, Columbia, SC, USA, <sup>2</sup>Mote Marine Laboratory and Aquarium, Sarasota, FL, USA, <sup>3</sup>ETH Zurich, Institute of Geochemistry and Petrology, Zürich, Switzerland

### Key Points:

- Lost City vent fluids are highly enriched in the short-lived radium isotope,  $^{223}\text{Ra}$ , but not in longer-lived  $^{226}\text{Ra}$  and  $^{228}\text{Ra}$
- Radium adsorption from Lost City vent fluids to solids is very low, similar to basalt-hosted systems
- Residence times of fluids in Lost City serpentinite are constrained to less than 2 y

### Supporting Information:

Supporting Information may be found in the online version of this article.

### Correspondence to:

W. S. Moore,  
moore@geol.sc.edu

### Citation:

Moore, W. S., Frankle, J. D., Benitez-Nelson, C. R., Früh-Green, G. L., & Lang, S. Q. (2021). Activities of  $^{223}\text{Ra}$  and  $^{226}\text{Ra}$  in fluids from the Lost City Hydrothermal Field require short fluid residence times. *Journal of Geophysical Research: Oceans*, 126, e2021JC017886. <https://doi.org/10.1029/2021JC017886>

Received 9 AUG 2021  
Accepted 15 NOV 2021

**Abstract** The residence time of fluids circulating through deep-sea hydrothermal systems influences the extent of water-rock reactions and the flux of major and minor elements to the ocean. While the fluid residence times in numerous basaltic and gabbroic systems have been determined, those of the less studied ultramafic systems are currently unknown. Fluids that interact with mantle rocks have fundamentally different chemistries and therefore have unique influences on seawater chemistry. In this first investigation of radium isotopes in a serpentinite-hosted system, vent fluids were discovered to contain 10–100 times greater activities of  $^{223}\text{Ra}$  (half-life = 11.4 days) than observed in high-temperature basalt-hosted systems. The  $^{223}\text{Ra}$  activities of 10–109 dpm L<sup>-1</sup> produce  $^{223}\text{Ra}/^{226}\text{Ra}$  activity ratios ranging from 9 to 109. These extremely high  $^{223}\text{Ra}$  activities, which are accompanied by low activities of  $^{226}\text{Ra}$ , place significant constraints on fluid residence times and the adsorption coefficient of radium between fluid and rock. Our data constrain the nondimensional retardation factor ( $R$ ) to very low values between 1 and 4, reflecting the extent to which Ra is transported more slowly than fluids due to adsorption and other processes. These results suggest that the residence time of fluids in contact with serpentinite is less than 2 y and perhaps as low as 0.5 y. They are surprisingly similar to those of basalt-hosted systems. Thus, fluids in hydrothermal systems share similar hydrogeological characteristics despite differences in rock types, underlying porosity, and heat sources, enabling larger-scale models of hydrothermal biogeochemistry to be developed across systems.

**Plain Language Summary** The well-known “black smoker” hydrothermal systems occur at ocean spreading centers. High temperature (200°C–400°C) fluids in these systems pass through basalt, where they become both acidic and rich in metals. As they emerge on the seabed after a few years, they precipitate metal-rich chimneys. Lesser-known hydrothermal systems occur in serpentinite. These systems form as minerals found deep in the earth are uplifted to the seabed and exposed to seawater. Here chemical reactions at lower temperatures (100°C–200°C) occur that convert primary Fe-bearing minerals to serpentine, releasing hydrogen (H<sub>2</sub>) and producing alkaline fluids. These conditions allow simple carbon molecules to be converted to more complex molecules including, potentially, amino acids, without the assistance of living organisms. Once formed, these molecules slowly degrade. A fundamental question regarding serpentinite-hosted systems is whether the molecules can be exported to the seabed before they are destroyed. We discovered a rare radium isotope,  $^{223}\text{Ra}$  (half-life = 11 days), was much enriched compared to the more common  $^{226}\text{Ra}$  (half-life = 1,600 y) in fluids from the Lost City serpentinite-hosted system. This argues fluid circulation times of less than 2 y, likely short enough to allow complex molecules to be exported into overlying ocean waters.

## 1. Introduction

Seawater passing through hot oceanic crust initiates a series of reactions that play a significant role in controlling the concentrations and distributions of major ions and trace metals in the ocean. The chemistry of these hydrothermal fluids depends on multiple variables including rock type, temperature, degree of prior rock alteration, convective path length, the effective water/rock ratio, and flow rate (Kadko, 1996; Von Damm et al., 1985). The vast majority of identified marine hydrothermal systems are hosted in mafic rocks (basalt and gabbro), resulting in acidic fluids that are rich in metals. In contrast, fluids that pass through ultramafic rocks (peridotite, including harzburgite and dunite) trigger a water-rock reaction called serpentinitization that converts peridotite to serpentinite (a rock composed of one or more serpentine group minerals) and releases free hydrogen (H<sub>2</sub>) to high pH fluids. High concentrations of H<sub>2</sub> coupled with appropriate catalysts, can lead to the nonbiological synthesis of organic molecules including methane, formate, and short-chain hydrocarbons (Lang et al., 2018; McCollom & Seewald, 2007; Proskurowski et al., 2008). The continuous supply of H<sub>2</sub> and abiotic organic compounds may

© 2021. The Authors.

This is an open access article under the terms of the [Creative Commons Attribution-NonCommercial-NoDerivs License](https://creativecommons.org/licenses/by/4.0/), which permits use and distribution in any medium, provided the original work is properly cited, the use is non-commercial and no modifications or adaptations are made.

have created the conditions that ultimately allowed life to develop on Earth and/or on other planets (Martin & Russell, 2007; Sojo et al., 2016).

Physical properties such as density, porosity, and permeability can differ substantially between mafic and ultramafic rocks (Bayrakci et al., 2018; Titarenko & McCaig, 2016), suggesting that circulation pathways of fluids through ultramafic systems may also differ from mafic systems. Mafic black smoker hydrothermal systems are primarily heated by emplacement of magma (German & Von Damm, 2004) in contrast to ultramafic systems where fluid circulation can be largely driven by lithospheric heat (Allen & Seyfried, 2004). As such, parameters such as residence time and flow rate could also differ between the two systems. In mafic systems hot, buoyantly rising fluids discharge from depths of  $\sim 1\text{--}3$  km in relatively narrow, high permeability upflow zones (Fisher, 2004; McCaig et al., 2007); whereas grain boundary flow and/or pre-existing structural features may be more important in controlling fluid pathways in ultramafic systems (Kelley et al., 2005; Lang et al., 2021).

Multiple approaches have been used to constrain residence times in hydrothermal systems. Short lived radionuclides indicate that fluids circulate through high temperature ( $>200^\circ\text{C}$ ) black smoker fields relatively quickly,  $<3$  y (Kadko, 1996). In contrast, low temperature ( $63^\circ\text{C}$ ) fluids that pass through 2–5 Ma crust on the Juan de Fuca ridge flank travel longer distances in the crust and have longer residence times. On the Juan de Fuca ridge flank, seawater enters the crust via a seamount approximately 52 km from a site of hydrothermal discharge (Fisher et al., 2003; Wheat et al., 2000). If transport rates determined from an injected tracer ( $\sim 2\text{--}3$  m  $\text{d}^{-1}$ ; Neira et al., 2016) apply to hydrothermal transport from the site of downwelling to the site of discharge, it would translate to a travel time of  $\sim 60$  y. Tracer transport times and fluid residence times are not necessarily directly comparable as tracer studies reflect the age of the fastest moving fluids while radionuclide ages reflect the age across the mean life of the radionuclide, including diffusive loss to dead zones, adsorption-desorption reactions during lateral transport, and mixing with older trapped water masses (Bethke & Johnson, 2002). Nonetheless, both provide important constraints on how fluids move in the subseafloor.

Fluid residence times will govern the abundances of chemical constituents with slower reaction times. For example, hot chemically reduced hydrothermal fluids mix locally with cold, oxidized seawater that is drawn into the subsurface (Bemis et al., 2012). The resulting “diffuse” fluids span temperature ranges from  $4^\circ\text{C}$  to  $>150^\circ\text{C}$  and have relatively brief crustal residence times of  $<3$  y (Kadko, 1996). In these shallow subseafloor mixing regimes, extremely reactive constituents, such as  $\text{H}_2$  and formate, are consumed or produced before the fluids again exit the seafloor (Lang et al., 2018; McDermott et al., 2020; Von Damm & Lilley, 2004; Wankel et al., 2011). Other chemical species, such as magnesium ( $\text{Mg}^{2+}$ ), are hardly affected as they react slowly, if at all at  $<150^\circ\text{C}$ . In contrast, fluids on the Juan de Fuca ridge flank have zero  $\text{Mg}^{2+}$  despite having similar temperatures ( $62^\circ\text{C}$ ; Mottl et al., 1998) because these fluids reside in the crust for sufficient time for the water-rock reactions governing  $\text{Mg}^{2+}$  removal to proceed. If residence times in ultramafic systems are substantially different than in magmatic systems, they will have implications for the assemblage of inorganic and biogeochemical reactions that can occur.

The Lost City Hydrothermal Field (LCHF;  $30^\circ\text{N}$ , Mid-Atlantic Ridge) is an iconic example of an ultramafic system (Kelley et al., 2005). Fluid, chimney, and rock samples were collected in September 2018 and  $^{223}\text{Ra}$ ,  $^{226}\text{Ra}$ , and  $^{228}\text{Ra}$  activities measured along with fluid chemistry. Unlike mafic systems, which contain radium isotope ratios similar to their production ratios from uranium isotopes in basalt (Kadko & Butterfield, 1998), fluids from LCHF have  $^{223}\text{Ra}/^{226}\text{Ra}$  activity ratios (ARs) over 2,000 times greater than expected from the parent U isotopes ( $^{235}\text{U}/^{234}\text{U}$ ) in ultramafic rocks. The discovery of exceptionally high  $^{223}\text{Ra}$  (half-life = 11.4 days) activities in fluids from the LCHF provides a powerful tool to constrain residence times of fluids in this system. Models developed for groundwater and mafic hydrothermal systems were adapted to translate the radium data into residence times. Sensitivity analyses were used to test assumptions inherent in the models. Our results indicate that the residence times of fluids in serpentinite below the LCHF must be a few years or less.

## 2. Methods

### 2.1. Study Site

The Lost City Hydrothermal Field lies on a terrace at the top of the southern ridge of the Atlantic Massif and hosts a variety of hydrothermal vents with warm ( $40^\circ\text{C}$ – $90^\circ\text{C}$ ), high pH (9–11) fluids (Kelley et al., 2001; Figure 1). The Atlantic Massif is an oceanic core complex consisting of gabbro and peridotite which was emplaced 1.5–2 My ago (Cann et al., 1997; Karson et al., 2006). The LCHF has been venting for at least 35 Ky (Früh-Green

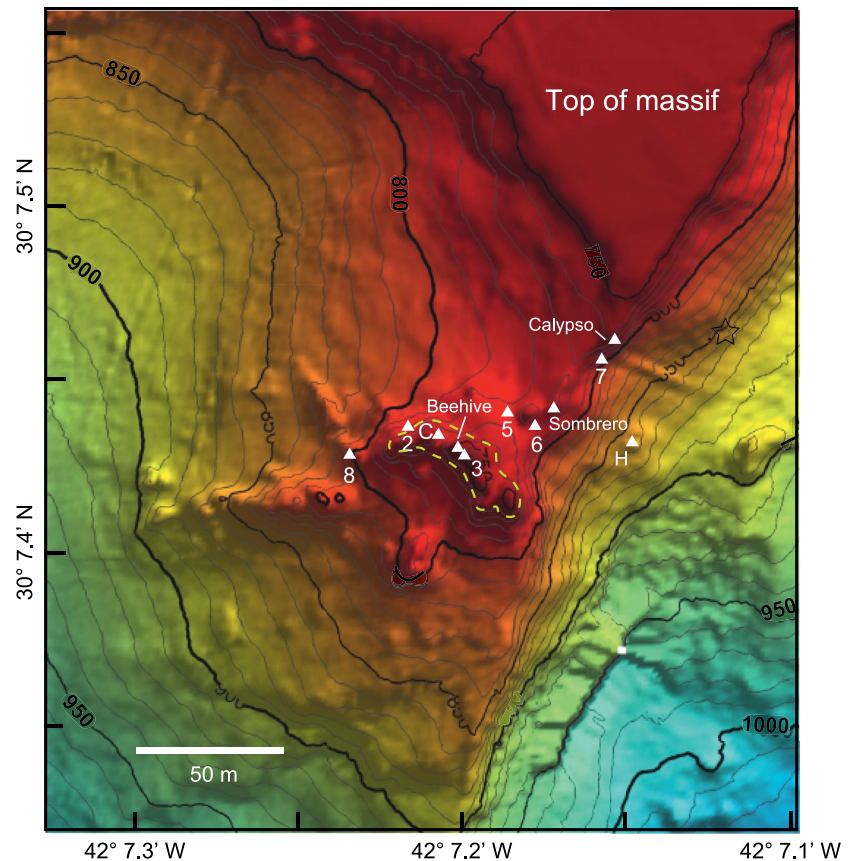


**Figure 1.** Map of the Lost City Hydrothermal Field (30°N, Mid-Atlantic Ridge). Actively venting chimneys are designated with white triangles. Depth contours are in meters. Vents at Beehive and Markers 2, 3 and C are on the Poseidon complex, which is outlined with a yellow dashed line. Adapted from Kelley et al. (2005).

et al., 2003; Kelley et al., 2001), and possibly as long as 120 Ky (Ludwig et al., 2011), as peridotite is continually converted to serpentinite. As the hydrothermal fluids mix with seawater, varying proportions of calcium carbonate and brucite are deposited, forming spectacular towers up to 60 m high that vent fluids at various depths (Kelley et al., 2001). The LCHF is interpreted to be the surface expression of fluids emanating from fault zones that tap a region of active serpentinization in the underlying peridotites (Kelley et al., 2005).

The Poseidon complex dominates the center of the field. It is a monolithic, 60-m-tall brucite-carbonate edifice, and hosts multiple distinct venting chimneys including those with the hottest temperature fluids. Four large columns coalesce at their base to form a composite structure, with fluids exiting from parasitic chimneys and actively venting flanges at multiple locations (Kelley et al., 2005).

## 2.2. Shipboard Fluid Sample Collection, Processing and Analysis

Fluid samples from the LCHF were collected in September 2018 during the AT42-01 expedition of the R/V Atlantis with the remotely operated vehicle (ROV) Jason II using the Hydrothermal Organic Geochemistry sampler that shunts fluid from a titanium intake into pre-cleaned Kynar® bags (Lang & Benitez-Nelson, 2021).

Radium from two unfiltered samples was concentrated at sea by BaSO<sub>4</sub> precipitation and analyzed onshore by gamma spectrometry (Van Der Loeff & Moore, 1999). Six additional unfiltered samples were analyzed onshore by RaDeCC (Moore & Arnold, 1996) after extraction onto Mn-fiber (Moore, 1976, 2008). Detailed descriptions of fluid collection, processing, and analytical techniques are in the Extended Method section of SI.

**Table 1**  
Geochemical Data for Fluid Samples

Sample name	Vent	Depth (m)	Avg. temp. (°C)	Highest temp. (°C)	pH	Volume (L)	Mg (mM)
J2-1110-LV16-G	Marker C	779	74.7	79.7	10.1	0.500	5.9
J2-1111-LV16-G	Sombrero	762	50.1	61.6	9.1	0.500	25.7
J2-1111-LV16	Sombrero	762	50.1	61.6	9.1	0.445	25.7
J2-1107-CHEM7	Marker 2	764	46.8	58.3	10.1	0.300	21.8
J2-1108-CHEM3	Beehive	743	95.4	95.6	10.8	0.300	0.4
J2-1110-CHEM5	Marker 8	801	34.8	52.6	9.9	0.345	14.5
J2-1111-CHEM4	Marker 3	731	--	85.0	9.0	0.175	26.6
J2-1108-CHEM7	Calypso	798	31.7	32.9	9.4	0.100	31.4

Note. "--" represents no data.

### 2.3. Solid Sample Collection and Analysis

Samples of serpentinite, gabbro, and carbonate-brucite collected during the 2018 expedition and obtained from archived sources were analyzed for  $^{238}\text{U}$ ,  $^{232}\text{Th}$ ,  $^{226}\text{Ra}$ ,  $^{228}\text{Ra}$ ,  $^{228}\text{Th}$ , and  $^{227}\text{Ac}$  using a combination of ICP-MS and gamma spectrometry (Moore, 1984). Detailed descriptions of rock collection and analytical techniques are in the Extended Method section of SI.

### 2.4. Radon Emanation Experiments

If  $^{223}\text{Ra}$  ( $^{227}\text{Ac}$ ) and  $^{224}\text{Ra}$  ( $^{228}\text{Th}$ ) are located near particle surfaces,  $^{219}\text{Rn}$  and  $^{220}\text{Rn}$  emanations are expected to occur as they are produced by alpha recoil. Additional analyses were therefore carried out to determine the portion of  $^{223}\text{Ra}$  and  $^{224}\text{Ra}$  near particle surfaces using the procedure of Cai et al. (2012) and Maiti et al. (2015). In brief, an aliquot of the crushed sample (7–17 g) was spread into a thin layer onto a GF/F filter in a plastic holder and dampened with de-ionized water to facilitate emanation. The direct emanation out of the solid of  $^{219}\text{Rn}$  from  $^{223}\text{Ra}$  and  $^{220}\text{Rn}$  from  $^{224}\text{Ra}$  was measured by RaDeCC. The measurement of each sample was repeated one to four times. Background/blanks were measured by counting the empty sample holders and filters overnight. The background/blanks for the  $^{220}\text{Rn}$  measurements were not significantly different from the samples and the results are therefore not reported. The  $^{219}\text{Rn}$  measurements are blank-corrected using a blank of  $0.003 \pm 0.003$  cpm.

## 3. Results

### 3.1. Fluids

Sample descriptions and geochemical parameters are given in Table 1.

Two exploratory samples were processed at sea and measured by gamma spectrometry (Table 2). The sample from Marker C (See Figure 1 for vent locations.) had an extremely high  $^{223}\text{Ra}_w$  activity ( $96.9 \text{ dpm L}^{-1}$ , see Figure S1), low  $^{226}\text{Ra}_w$  activity ( $0.9 \text{ dpm L}^{-1}$ ), and no detectable  $^{228}\text{Ra}_w$ . The sample from Sombrero had lower, but easily measurable,  $^{223}\text{Ra}_w$  activity ( $9.5 \text{ dpm L}^{-1}$ ), low  $^{226}\text{Ra}_w$  ( $0.65 \text{ dpm L}^{-1}$ ), and no detectable  $^{228}\text{Ra}_w$ . The high activities of  $^{223}\text{Ra}_w$  in these exploratory samples were verified by measuring six additional fluid samples by RaDeCC (Table 2). The activities of  $^{223}\text{Ra}_w$  in these additional fluids ranged from 5 to  $35 \text{ dpm L}^{-1}$  except for the sample from Marker 3, where it was below the detection limit (0 counts in 1,200 min). Duplicate samples from Sombrero, although measured by different techniques, had  $^{223}\text{Ra}_w$  activities that agreed to within  $\pm 6\%$  and  $^{226}\text{Ra}_w$  activities that agreed to within  $\pm 8\%$  (Table 2).

After complete decay of  $^{223}\text{Ra}_w$ , the six fluid samples were re-analyzed by RaDeCC at least three months later and found to have barely detectable  $^{227}\text{Ac}_w$  in only three samples ( $0.007\text{--}0.017 \text{ dpm L}^{-1}$ ) indicating  $^{223}\text{Ra}_w$  was largely unsupported from parent decay in the vent fluids (Table 2). Because the samples run on the RaDeCC were all older than 35 days, any  $^{224}\text{Ra}_w$  activity, if present, would have decreased to  $\sim 0.001\%$  of in situ values, well below the limit of detection.

**Table 2**  
*Measured and Calculated Endmember Activities (dpm L<sup>-1</sup>)*

Sample	Vent	Measured				Calculated fluid endmembers		
		<sup>223</sup> Ra <sub>w</sub>	<sup>226</sup> Ra <sub>w</sub>	<sup>227</sup> Ac <sub>w</sub> **	<sup>228</sup> Th <sub>w</sub> **	<sup>223</sup> Ra <sub>w</sub>	<sup>226</sup> Ra <sub>w</sub>	<sup>223</sup> Ra <sub>w</sub> / <sup>226</sup> Ra <sub>w</sub> AR
J2-1110-LV16-G	Marker C	96.9 ± 3.0	0.9 ± 0.1	Bdl	Bdl	109	0.9	109
J2-1111-LV16-G	Sombrero	9.5 ± 1.3	0.7 ± 0.1	Bdl	Bdl	18	1.2	14
J2-1111-LV16	Sombrero	8.9 ± 0.4	0.7 ± 0.1	Bdl	0.10	17	1.2	13
J2-1107-CHEM7	Marker 2	35.5 ± 2.0	0.9 ± 0.1	0.017	0.08	60	1.4	39
J2-1108-CHEM3	Beehive	20.0 ± 0.7	1.4 ± 0.1	0.007	0.28	20	1.3	14
J2-1110-CHEM5	Marker 8	6.8 ± 0.8	0.7 ± 0.1	0.009	0.15	*	*	*
J2-1111-CHEM4	Marker 3	Bdl	1.1 ± 0.1	0.004	0.35	Bdl	2.1	Bdl
J2-1108-CHEM7	Calypso	5.1 ± 0.3	2.5 ± 0.1	Bdl	0.82	*	*	*

*Note.* The first two samples were processed at sea and <sup>223</sup>Ra<sub>w</sub> activity was determined by gamma spectrometry (-G). Six additional samples were processed onshore and <sup>223</sup>Ra<sub>w</sub> was determined by RaDeCC. All <sup>226</sup>Ra<sub>w</sub> values were determined by gamma spectrometry. <sup>227</sup>Ac<sub>w</sub> and <sup>228</sup>Th<sub>w</sub> were determined by RaDeCC. Fluid endmember activities were corrected for seawater entrainment based on seawater Mg<sup>2+</sup> concentration (52.3 mM) and <sup>226</sup>Ra activity (0.1 dpm L<sup>-1</sup>) at this depth. Errors are expressed as 1σ. Some samples were likely contaminated by particles (\*), others were based on very few net counts (\*\*). Some sample measurements were below detection level (Bdl).

The <sup>226</sup>Ra<sub>w</sub> activities ranged from 0.7 to 2.5 dpm L<sup>-1</sup> (Table 2). We suspect that some of the <sup>226</sup>Ra activities may be due to release of <sup>226</sup>Ra from particles that were incorporated into the sample prior to processing (Markers 3 and 8 and Calypso, see Section 2.4; SI).

Samples had <sup>228</sup>Th activities that ranged from 0.08 to 0.82 dpm L<sup>-1</sup>. We suspect the higher activities are due to contamination by the carbonate particles (see Section 2.4; SI).

Reported errors for <sup>223</sup>Ra<sub>w</sub> (Table 2) are estimated from the error of the measurement of each sample based on the standard deviation of the multiple counts over 2–60 days after correcting for radioactive decay. These errors ranged from 1.4% to 12% (average = 5.3%) and are not significantly different from the estimated error using total net counts (100–600 counts per run). Measurements of <sup>226</sup>Ra<sub>w</sub> are based on four-to eight-day gamma counts conducted at least three months after the samples were precipitated with BaSO<sub>4</sub> after the initial <sup>223</sup>Ra had completely decayed. The error was estimated by the program, HYPERMET (Phillips & Marlow, 1976), based on the best fit to the 351 keV peak. The RaDeCC measurements of <sup>227</sup>Ac<sub>w</sub> and <sup>228</sup>Th<sub>w</sub> were based on 900–1600 min counts made five months after sample collection. For <sup>227</sup>Ac, 0–3 net counts were recorded; for <sup>228</sup>Th, 9–50 net counts were recorded. Errors were not placed on such small numbers as this would imply an accuracy that may not be warranted.

The final radionuclide activities were converted to fluid endmember activities using the Mg<sup>2+</sup> concentrations and assuming the endmembers contained no Mg<sup>2+</sup> and seawater contained 52.3 mM (Table 2). A further correction to the extrapolated endmember hydrothermal fluid values subtracted the activity of radium from adjacent seawater at this depth, which has activities that are below detection for <sup>223</sup>Ra and 0.1 dpm L<sup>-1</sup> for <sup>226</sup>Ra (Charette et al., 2015). These corrections provide our best estimate of radium contributed to the fluids from the rocks.

### 3.2. Radionuclides and Geochemistry of Solid Samples

Solid samples of serpentinites ( $n = 19$ ), gabbros ( $n = 4$ ), and the carbonate-brucite chimneys ( $n = 7$ ) were analyzed for <sup>226</sup>Ra, <sup>228</sup>Ra, <sup>238</sup>U, and <sup>232</sup>Th (Table S1).

There was a significant enrichment of <sup>238</sup>U<sub>r</sub> in the serpentinites (up to 1,300 dpm kg<sup>-1</sup> or 1.8 μg g<sup>-1</sup>) and carbonate-brucite chimneys (up to 8,350 dpm kg<sup>-1</sup> or 11.8 μg g<sup>-1</sup>) compared to unaltered ultramafic rocks (0.70–14 dpm kg<sup>-1</sup> or 0.001–0.02 μg g<sup>-1</sup>; Seitz & Hart, 1973) or gabbros (~7.75 dpm kg<sup>-1</sup> or 0.011 μg g<sup>-1</sup>; Godard et al., 2009). Uranium (U) concentrations measured by gamma spectrometry (<sup>234</sup>Th peak at 63 keV) or by ICP-MS as part of this work, as well as previously reported values by Boschi et al. (2006) were similar (Table S1). Discrepancies are largely due to the lower detection limit and higher precision of the ICP-MS.

**Table 3**  
Emanation Efficiency of  $^{219}\text{Rn}$  From Serpentine

Sample	$^{238}\text{U}$	$^{231}\text{Pa}^*$	$^{219}\text{Rn}$ emanation	Emanation efficiency
3,638–1,009	588	13.2	12.2	1.08
3,652–1,226	589	13.2	3.1	0.23
357 71A 1R2 11-18 cm U	548	12.5	2.8	0.22
357 69A 9R2 118-124 cm U	734	16.5	3.8	0.23

Note. Activities are  $\text{dpm kg}^{-1}$ .  $^{231}\text{Pa}$  is estimated based on a 35 Ky sample with  $^{235}\text{U}/^{238}\text{U}$  AR = 0.046.

Both serpentinites and the carbonate-brucite towers contained low concentrations of  $^{232}\text{Th}_r$  ( $\leq 42 \text{ dpm kg}^{-1}$  or  $0.17 \mu\text{g g}^{-1}$ ) as measured by ICP-MS. Both  $^{228}\text{Ra}_r$  and  $^{228}\text{Th}_r$  were only detected in three samples as measured by gamma spectrometry. The  $^{226}\text{Ra}_r$  activities varied widely within and among rock types (serpentinites:  $<60\text{--}1,160 \text{ dpm kg}^{-1}$ , carbonates:  $<60\text{--}1,700 \text{ dpm kg}^{-1}$ , gabbros:  $<60\text{--}550 \text{ dpm kg}^{-1}$ ) as measured by gamma spectrometry.

### 3.3. Emanation Efficiency of $^{223}\text{Ra}_r$ From Serpentine

The emanation experiments yielded very low values for  $^{219}\text{Rn}$ , requiring a careful assessment of the blank. RaDeCC measurements of empty sample holders recorded  $^{219}\text{Rn}$  count rates of  $0.003 \pm 0.003 \text{ cpm}$  ( $2\sigma$ ) and  $^{220}\text{Rn}$  count rates of  $0.026 \pm 0.014 \text{ cpm}$  ( $2\sigma$ ). Because each sample measurement (usually  $\sim 1,000 \text{ min}$ ) yielded very few counts of  $^{219}\text{Rn}$  for serpentinites (0–77), multiple measurements were blank corrected and then combined into a single value. Many samples (16 of 20) yielded count rates within the error of the blank; these are designated as Bdl. This left only four serpentine samples where U concentrations could be paired with finite  $^{219}\text{Rn}$  emanation values to estimate emanation efficiencies (Table 3).

Measurements were blank corrected and then combined into a single value. Many samples (16 of 20) yielded count rates within the error of the blank; these are designated as Bdl. This left only four serpentine samples where U concentrations could be paired with finite  $^{219}\text{Rn}$  emanation values to estimate emanation efficiencies (Table 3).

## 4. Discussion

The fluid samples from Lost City Hydrothermal Field have  $^{223}\text{Ra}$  activities that are much greater than any previous measurements in the ocean (Charette et al., 2015; Kipp et al., 2018; Neuholz et al., 2020). These high  $^{223}\text{Ra}$  activities are not accompanied by high activities of the other radium isotopes. Unlike samples from high-temperature vents, which have  $^{223}\text{Ra}/^{226}\text{Ra}$  AR's of 0.06–0.07 (Kipp et al., 2018; Neuholz et al., 2020), the LCHF samples have  $^{223}\text{Ra}/^{226}\text{Ra}$  AR's between 13 and 109. This is entirely unexpected because the parents of  $^{223}\text{Ra}$  ( $^{235}\text{U}$  and  $^{231}\text{Pa}$ ) normally have a factor of 20 lower activity than the  $^{226}\text{Ra}$  parents ( $^{238}\text{U}$ ,  $^{234}\text{U}$ , and  $^{230}\text{Th}$ ) in most oceanic rocks. No  $^{228}\text{Ra}$  (half-life = 5.7 y) activity was detected ( $<1 \text{ dpm L}^{-1}$ ) in any of the samples despite reaching abundances of as high as  $54 \text{ dpm L}^{-1}$  in some mafic hydrothermal systems (Kadko & Butterfield, 1998). Likewise,  $^{227}\text{Ac}$  was extremely low ( $0.007\text{--}0.017 \text{ dpm L}^{-1}$ ) in the three samples in which it was detected. This contrasts with estimated activities of  $15\text{--}22 \text{ dpm L}^{-1}$  in hydrothermal fluids from the TAG hydrothermal field (Kipp et al., 2015). Both the extremely high  $^{223}\text{Ra}$  activities and the high  $^{223}\text{Ra}/^{226}\text{Ra}$  AR's must therefore be explained.

In the following sections, we argue that the carbonate-brucite towers are not the source of the high measured  $^{223}\text{Ra}$  activities. Instead, we propose that the elevated  $^{223}\text{Ra}$  values measured here result from interaction with serpentinites that have unusually high  $^{235}\text{U}_r$  and  $^{238}\text{U}_r$  contents compared to other crustal rocks due to their extensive interaction with seawater (Figure 2). The  $^{223}\text{Ra}_w/^{226}\text{Ra}_w$  AR provides a constraint on the residence time of fluids in the crust, while the relationships of  $\text{Ra}_w$  and temperature have implications for subsurface fluid flow.

### 4.1. Fluids From the Poseidon Complex Exclude the Carbonate-Brucite Towers as the Source of the $^{223}\text{Ra}_w$

Fluids from four locations on the central Poseidon structure were sampled for Ra, at depths from 731 to 779 meters below the surface (mbs) (Markers C, 2, 3, and Beehive; Table 1; Figure 3). Fluids from Marker 3 are unusual as they are impacted by mixing with seawater that has been locally entrained and heated prior to venting (Lang et al., 2018; Lowell, 2017); this sample is therefore not considered further. After correcting for the  $\text{Mg}^{2+}$  content,  $^{223}\text{Ra}_w$  was highest in fluids venting closest to the seafloor and decreased in fluids higher up the complex (Figure 3). These data ( $^{223}\text{Ra}_w$  vs. mbs) can be fit to either a linear or exponential curve; both have  $R^2 = 0.97$ , meaning either mixing or decay (or a combination) describes the decline in  $^{223}\text{Ra}_w$  as the fluid moves through the chimney.

It might be expected that the shallowest fluids are also the coldest as they would have had more time to undergo conductive cooling. This is not the case as the hottest fluids are from the shallowest vent, Beehive (743 m,  $95.4^\circ\text{C}$ ). Markers C and 2 are large flange structures, however, and fluids were sampled from where they pooled below a large ledge. These fluids may have cooled rapidly at this late stage or could have undergone more conductive cooling during transport through the chimney due to the complex hydrology of the system.

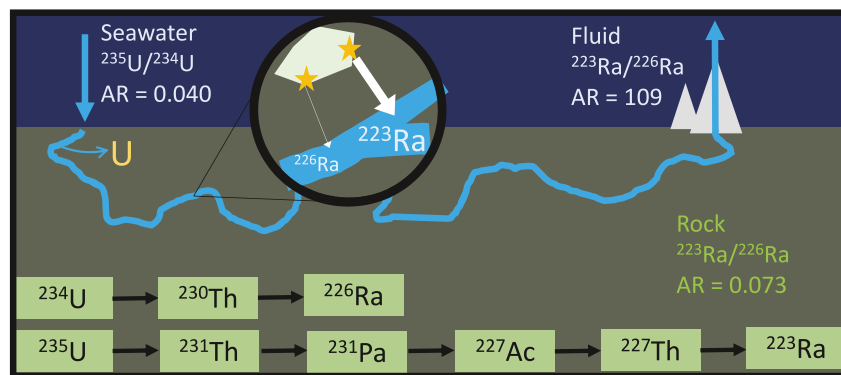


**Figure 2.** Hypothesized example of fluids circulating through an ultramafic system resulting in high  $^{223}\text{Ra}$  activities at an age of 35 Ky. Uranium (U) from seawater is deposited into the ultramafic surface as peridotite hydrates to serpentinite throughout the lifetime of the system (Michard & Albarede, 1985; Seitz & Hart, 1973; see Section 4.2). Over time the seawater derived  $^{235}\text{U}$  decays to  $^{223}\text{Ra}$  and  $^{234}\text{U}$  decays to  $^{226}\text{Ra}$ . If radium is removed from the serpentinite, the rate of regeneration of  $^{223}\text{Ra}$  is much faster than that of  $^{226}\text{Ra}$ , leading to a high  $^{223}\text{Ra}/^{226}\text{Ra}$  activity ratio (AR). The preservation of these high AR signatures in the exported fluids indicates there is very low adsorption of radium to the rock, which would otherwise cause the  $^{223}\text{Ra}$  to decay before being transported. Throughout this process serpentinization is ongoing and new seawater U is continually deposited, resulting in rocks at all stages to be currently present.

One clear outcome of these data is that the source of the  $^{223}\text{Ra}$  is not the carbonate-brucite towers themselves. If  $^{223}\text{Ra}$  was being released from the chimney deposits, we would expect fluids that traveled through more carbonate/brucite to acquire more  $^{223}\text{Ra}_w$ . The opposite occurred here. This is interpreted to mean the fluids emerging from the serpentinite have high  $^{223}\text{Ra}_w$  activities and that these activities decrease as fluids move through the chimney due to radioactive decay and potentially mixing with packets of older water. These data unfortunately cannot be converted to fluid velocities since the observed loss of  $^{223}\text{Ra}_w$  may also reflect the potential minor inputs from the carbonate (which would make fluid velocities appear slower) and removal due to adsorption (which would make the fluid velocities appear faster).

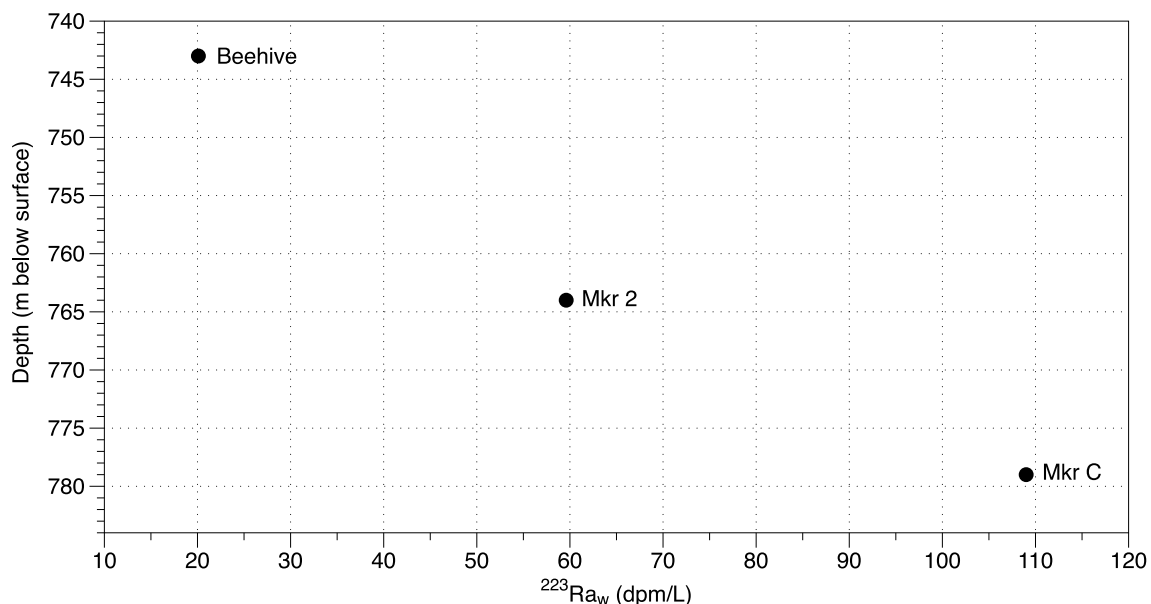


**Figure 3.**  $^{223}\text{Ra}_w$  of fluids from vents at different depths on the Poseidon complex show higher activities near the base of the structure.

#### 4.2. Uranium and Thorium Concentrations and Activity Ratios in Serpentinites

Peridotite, the precursor of serpentine, has very low concentrations of U, on the order of 0.001–0.02  $\mu\text{g g}^{-1}$  (Seitz & Hart, 1973). However, serpentinites have much higher U abundances due to the incorporation of seawater U during the hydration reaction (Seitz & Hart, 1973). At the Atlantis Massif serpentinites have U concentrations that range from 0.02 to 5.1  $\mu\text{g g}^{-1}$  (14–3,600 dpm  $\text{kg}^{-1}$ ; Boschi et al., 2006; Früh-Green et al., 2018; Table S1). These U concentrations were determined in 23 grab samples from the south wall of the Atlantis Massif where the LCHF is located (Boschi et al., 2006; this work) and in seven shallow (<2 m) drill cores acquired during IODP Expedition 357 (Früh-Green et al., 2018). Combined, U concentrations averaged  $1.1 \pm 1.3 \mu\text{g g}^{-1}$  ( $775 \pm 916$  dpm  $\text{kg}^{-1}$ ; Table S1).

The average  $^{235}\text{U}/^{238}\text{U}$  and  $^{234}\text{U}/^{238}\text{U}$  ARs in seawater are 0.046 and 1.14, respectively (Chen et al., 1986). Dividing these values, we expect the seawater-derived U in serpentine to have an initial  $^{235}\text{U}/^{234}\text{U}$  AR of 0.040. With time,  $^{234}\text{U}$  (half-life = 245 Ky) produces  $^{230}\text{Th}$  (half-life = 75 Ky), the immediate parent of  $^{226}\text{Ra}$ . Likewise,  $^{235}\text{U}$  (half-life = 704 My) produces  $^{231}\text{Pa}$  (half-life = 34 Ky), which decays to  $^{227}\text{Ac}$  (half-life = 21.7 y) and  $^{227}\text{Th}$  (half-life = 18.6 days), the immediate parent of  $^{223}\text{Ra}$ . The change in the  $^{231}\text{Pa}/^{230}\text{Th}$  AR with time is shown in Figure S2.

Samples measured for  $^{232}\text{Th}$ , the immediate parent of another radium isotope,  $^{228}\text{Ra}$  (half-life = 5.75 y) had an average concentration of  $7 \pm 13$  dpm  $\text{kg}^{-1}$  ( $0.03 \pm 0.05 \mu\text{g g}^{-1}$ ; Table S1), consistent with low Th abundance in mafic and ultramafic rocks (Seitz & Hart, 1973). Because seawater has extremely low activities of  $^{230}\text{Th}$ ,  $^{232}\text{Th}$ , and  $^{231}\text{Pa}$  compared to U (Moore & Sackett, 1964), these radionuclides are not significantly enriched in the serpentine by seawater interactions.

#### 4.3. Production of $^{223}\text{Ra}$ and $^{226}\text{Ra}$ From Serpentinites

The production of  $^{223}\text{Ra}$  and  $^{226}\text{Ra}$  depends not only on the  $^{234}\text{U}$  and  $^{235}\text{U}$  content of the host rock but also the amount of time available for ingrowth of  $^{231}\text{Pa}$  and  $^{230}\text{Th}$ . The uplift of the Atlantis Massif began at least 1.5 My ago (Cann et al., 1997; Karson et al., 2006). Since then, the system has continued to evolve as seawater continuously converts peridotite to serpentine and other rocks. The LCHF is at least 35 Ky based on  $^{14}\text{C}$  dating of the carbonate structures (Früh-Green et al., 2003) and may be >120 Ky based on  $^{230}\text{Th}$  dating (Ludwig et al., 2011). Thus, there has been adequate time for considerable generation of  $^{230}\text{Th}$  and  $^{231}\text{Pa}$  in the serpentine.

Variable serpentine ages will lead to slight differences in the production ratios of  $^{223}\text{Ra}/^{226}\text{Ra}$  in the rocks. For example, in a 35 Ky old serpentine, ingrowth results in  $^{230}\text{Th}$  activities that are 28% of the  $^{234}\text{U}$  activity. Over this time,  $^{231}\text{Pa}$  reaches about 51% of the  $^{235}\text{U}$  activity, resulting in a  $^{223}\text{Ra}_r/^{226}\text{Ra}_r$  AR of 0.073 (Figure S2). Because the LCHF system continues to evolve, some serpentinites will be substantially younger than 35 Ky, while others may be older. Young (5 Ky) serpentinites will have the maximum  $^{223}\text{Ra}_r/^{226}\text{Ra}_r$  AR of 0.085. After 500 Ky the minimum AR of 0.04 is reached. The minor effect of excess  $^{234}\text{U}$  decay since being incorporated from seawater was not included in the calculations. For initial calculations, we use a  $^{223}\text{Ra}_r/^{226}\text{Ra}_r$  AR at 35 Ky of 0.073, recognizing it could be slightly higher or lower.

Given low  $^{223}\text{Ra}_r/^{226}\text{Ra}_r$  AR of <0.1 in the rocks, why do the LCHF fluids have  $^{223}\text{Ra}_w/^{226}\text{Ra}_w > 10$ ? The answer must lie in part with the difference in their regeneration times. When Ra is leached from a rock, each isotope regenerates at a rate based on its decay constant. For  $^{223}\text{Ra}$  and  $^{226}\text{Ra}$ , the ratio of decay constants is:

$$\frac{\lambda_{223}}{\lambda_{226}} = \frac{6.08 \times 10^{-2} \text{d}^{-1}}{1.18 \times 10^{-6} \text{d}^{-1}} = 5.2 \times 10^4 \quad (1)$$

In other words, in a system initially free of radium,  $^{223}\text{Ra}$  regenerates over 50,000 times faster than  $^{226}\text{Ra}$ . Thus, depending on the adsorption of radium to solid surfaces, there is the potential for substantially more  $^{223}\text{Ra}$  to be released into the vent fluid relative to  $^{226}\text{Ra}$ . Below, we exploit the differences in  $^{223}\text{Ra}$  and  $^{226}\text{Ra}$  regeneration rates to calculate fluid residence times.



#### 4.4. Models for $^{223}\text{Ra}$ and $^{226}\text{Ra}$ in Vent Waters to Constrain Residence Times

A large body of work has established the use of  $^{210}\text{Pb}$ ,  $^{222}\text{Rn}$ ,  $^{228}\text{Ra}$ , and  $^{226}\text{Ra}$  to study the residence time of fluids in hydrothermal systems (Kadko, 1996; Kadko et al., 1985/86; Kadko & Moore, 1988). These models were developed in basalt-hosted systems, where low pH conditions (2–3) minimized surface adsorption of radium onto solids as it was released from the rock matrix and into solution by rock alteration and by alpha recoil. In contrast, the high pH conditions (9–11) in serpentinite-hosted systems require that adsorption onto solid surfaces be considered. At the same time, however, high pH conditions also reduce the potential of Ra release during rock alteration. Thus, the models previously applied to estimate residence times in hydrothermal systems are not directly applicable to the LCHF.

We developed a model for the LCHF based on studies of Ra in groundwater (e.g., Kiro et al., 2013, 2012; Krishnaswami et al., 1982; Rajaomahefasoa et al., 2019; Weinstein et al., 2021); terrestrial geothermal systems (Hammond et al., 1988); and marine hydrothermal systems (Cochran & Kadko, 2008). Our model assumes: (a) more than 99% of the U in the serpentinite was deposited from seawater as the serpentinite formed (Seitz & Hart, 1973), (b) the serpentinite at the LCHF formed at least 5 Ky ago and possibly as early as 1 My (Kelley et al., 2001, 2005), (c) the only source of radium into the fluids is from the serpentinite and is due to alpha recoil from  $^{230}\text{Th}$  and  $^{231}\text{Pa}$  daughters that have been generated through U decay, and (d) the system is at steady state on a time scale of a few years. In this model, any additional radium released from the rock due to alteration after serpentinite formation is neglected. The validity of this simplifying assumption is considered in Section 4.4.3.

##### 4.4.1. Maximum Residence Time Constrained by $^{223}\text{Ra}/^{226}\text{Ra}$ Activity Ratios

We start with an equation from Rajaomahefasoa et al. (2019) developed for the production of mobile Ra isotopes in groundwater, neglecting rock alteration:

$$\text{Ra}_w = \frac{R_{e,i}}{\phi \lambda_i R} [1 - e^{-\lambda_i RT}] \text{Ra}_r \varphi_r + \text{Ra}_{w(0)} e^{-\lambda_i RT} \quad (2)$$

$\text{Ra}_w$  = dissolved radium in water (dpm  $\text{L}^{-1}$ ),

$\text{Ra}_{w(0)}$  = dissolved radium in water at  $t = 0$  (dpm  $\text{L}^{-1}$ ),

$R_{e,i}$  = recoil rate constant of isotope  $i$  ( $\text{y}^{-1}$ ),

$\lambda_i$  = the decay constant of isotope  $i$  ( $\text{y}^{-1}$ ),

$T$  = residence time of fluid, that is, the amount of time that the fluid is in contact with the rock (y),

$R$  = retardation factor (i.e., residence time of Ra/residence time of fluid). Dissolved Ra moves more slowly than the vent water due to adsorption, and  $R$  varies from a minimum of 1 (no adsorption) to a maximum of  $\infty$  (Ra is fully adsorbed). Note that  $R - 1 = K$ , the dimensionless adsorption coefficient (Krishnaswami et al., 1982),

$\text{Ra}_r$  = radium in rock (dpm  $\text{kg}^{-1}$ ),

$\varphi_r$  = rock density ( $\text{kg dm}^{-3}$ ),

$\phi$  = porosity.

In the second term,  $\text{Ra}_{w(0)}$  could be finite because when seawater interacts with peridotite it carries dissolved radium that may be incorporated into the fluids. This is not an issue with  $^{223}\text{Ra}$  because seawater activities are very much lower than fluid activities. For  $^{226}\text{Ra}$ , the seawater activity is about 10% of the fluid activity. Some of the seawater  $^{226}\text{Ra}$  is likely adsorbed before it reaches the serpentinite, so the 10% figure is a maximum. We have corrected the fluid  $^{226}\text{Ra}$  activity by subtracting the maximum initial activity that might be contributed from seawater. Thus,  $\text{Ra}_{w(0)} = 0$ .

Equations can be written for both  $^{223}\text{Ra}$  and  $^{226}\text{Ra}$ . Dividing these equations results in:

$$\frac{^{223}\text{Ra}_w}{^{226}\text{Ra}_w} = \frac{\frac{R_{e,223}}{\phi \lambda_{223} R} [1 - e^{-\lambda_{223} RT}] ^{223}\text{Ra}_r \varphi_r}{\frac{R_{e,226}}{\phi \lambda_{226} R} [1 - e^{-\lambda_{226} RT}] ^{226}\text{Ra}_r \varphi_r} \quad (3)$$

Note that both  $\phi_r$  and  $\phi$  cancel (see Section 4.4.2).

The recoil rate constant is related to the recoil efficiency ( $\epsilon$ , fraction of recoil events that displace the daughter toward the surface), the recoil range, and the characteristic rock surface, which is related to surface area (Rajaomahefasoa et al., 2019).

$$R_{e,i} = \epsilon \gamma \lambda_i S \quad (4)$$

$\epsilon$  = factor for recoil efficiency,

$\gamma$  = recoil range ( $\mu\text{m}$ ),

$S$  = extent of surface of rock in contact with a unit volume of water ( $\mu\text{m}^{-1}$ ).

The equation for each isotope is written and the equations are divided. Assuming  $\epsilon$ ,  $\gamma$ , and  $S$  are the same for the production of mobile  $^{223}\text{Ra}$  and  $^{226}\text{Ra}$ , the  $R_e$  ratio for  $^{223}\text{Ra}$  and  $^{226}\text{Ra}$  becomes:

$$\frac{R_{e,223}}{R_{e,226}} = \frac{\lambda_{223}}{\lambda_{226}} \quad (5)$$

These results in Equation 3 to now be rewritten as:

$$\frac{{}^{223}\text{Ra}_w}{{}^{226}\text{Ra}_w} = \frac{[1 - e^{-\lambda_{223}RT}] {}^{223}\text{Ra}_r}{[1 - e^{-\lambda_{226}RT}] {}^{226}\text{Ra}_r} \quad (6)$$

Since  $R \geq 1$ , the system attains equilibrium with respect to  $^{223}\text{Ra}$  within two months of the fluid being in contact with the rock, that is,  $[1 - e^{-\lambda_{223}RT}] {}^{223}\text{Ra}_r = {}^{223}\text{Ra}_r$ .

At 35 Ky serpentinites are expected to contain a  $\frac{{}^{223}\text{Ra}_r}{{}^{226}\text{Ra}_r} = 0.073$ , based on the expected  $\frac{{}^{231}\text{Pa}_r}{{}^{230}\text{Th}_r}$  in the rock (Section 4.1; Figure S2), thus:

$$\frac{{}^{223}\text{Ra}_w}{{}^{226}\text{Ra}_w} = \frac{0.073}{[1 - e^{-\lambda_{226}RT}]} \quad (7)$$

Our highest measured endmember value for  $\frac{{}^{223}\text{Ra}_w}{{}^{226}\text{Ra}_w} = 109$  (Table 2).

Earlier we adjusted for  $^{226}\text{Ra}$  in the seawater that contaminated the endmember fluid during collection. Here, we subtract the  $^{226}\text{Ra}$  in the seawater that produced the serpentines ( $0.1 \text{ dpm L}^{-1}$ ), raising the endmember AR to 121. Using this value, we can solve Equation 7 for  $RT$ :

$$RT = \frac{\left(-\ln\left(1 - \frac{0.073}{121}\right)\right)}{\lambda_{226}} = \frac{6.0 \times 10^{-4}}{4.33 \times 10^{-4} \text{ yr}^{-1}} = 1.4 \text{ y} \quad (8)$$

$$T = \frac{1.4\text{y}}{R} \quad (9)$$

At the minimum value of  $R$  ( $R = 1$ : no adsorption),  $T$  is its maximum value for 35 Ky old serpentinite, 1.4 y. Any adsorption will lead to lower values for  $T$ . Serpentinites older than 35 Ky will lead to smaller  $\frac{{}^{223}\text{Ra}_r}{{}^{226}\text{Ra}_r}$  and even lower  $T$  values (Figure S3). Even an extremely young age for the serpentinite of 5 Ky would only minimally increase the  $\frac{{}^{223}\text{Ra}_r}{{}^{226}\text{Ra}_r}$  to 0.085, resulting in a fluid residence time of 1.6 y at  $R = 1$ . Therefore, the maximum residence time of the fluids must be  $<2 \text{ y}$  (Figure 4).

We will now consider limits of  $R$  based on the  $^{223}\text{Ra}_w$  and  $^{226}\text{Ra}_w$  data.

#### 4.4.2. Retardation Factor Constrained by $^{223}\text{Ra}_w$

Emanation of radon (Rn) from rock requires its parent to be located near the grain's surface or connected to a pathway through which radon can readily migrate (Rama & Moore, 1990). This is especially true for  $^{219}\text{Rn}$  with only a 4 s half-life. Thus, the emanation of  $^{219}\text{Rn}$  should reflect the  $^{223}\text{Ra}_r$  atoms that are sufficiently close to the grain's surface that they could be lost to fluid in contact with the rock surface. Comparing  $^{219}\text{Rn}$  emanation with

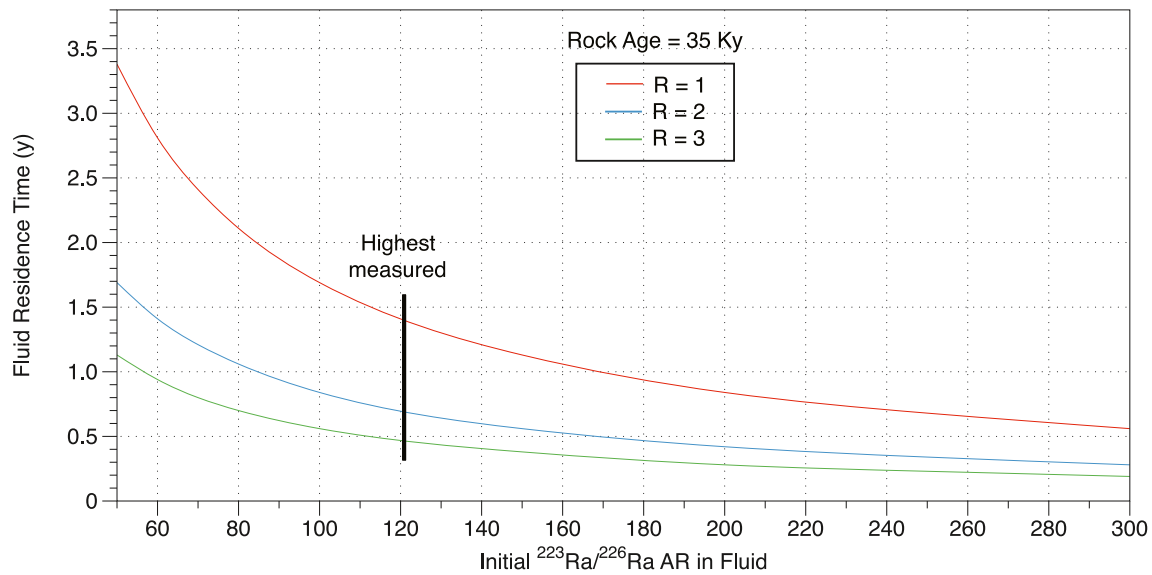


**Figure 4.** Variations in the fluid residence time ( $T$ ) for different values of retardation factors ( $R$ ) for a 35 Ky old serpentinite. The highest measured  $^{223}\text{Ra}/^{226}\text{Ra}$  AR in the fluid from Marker C after adjusting for  $^{226}\text{Ra}$  contributed by seawater corresponds to a residence time between 0.5 and 1.4 y.

the  $^{231}\text{Pa}$  daughter activity of the rock should therefore provide a measure of the escape probability for  $^{223}\text{Ra}$  after recoil from  $^{227}\text{Th}$  decay. Cochran and Kadko (2008) presented a model to predict the production rate (atoms  $\text{L}^{-1} \text{min}^{-1}$ ) of mobile Ra in marine groundwaters:

$$P = A_p \times \frac{1}{\phi} \times \rho_w \times \alpha \quad (10)$$

where:

$P$  = production rate of mobile Ra (atoms  $\text{L}^{-1} \text{min}^{-1}$ ),

$A_p$  = activity of parent in rock (dpm  $\text{kg}^{-1}$ ),

$\phi$  = porosity (for LCHF = 0.038, Tutolo et al., 2016),

$\rho_w$  = density of fluid (1.02  $\text{kg L}^{-1}$ ),

$\alpha$  = recoil efficiency (atoms recoiled/atoms produced).

Values of  $\alpha$  for  $^{226}\text{Ra}$  range from 0.75 for deep sea clays, where almost all  $^{230}\text{Th}$  is adsorbed on the surface, to  $<0.01$  in rocks, where  $^{230}\text{Th}$  is within crystallized minerals (Cochran & Kadko, 2008). Kadko and Butterfield (1998) used a value of 0.2 for the recoil efficiency of  $^{224}\text{Ra}$  from basalts on the Juan de Fuca Ridge. Serpentine minerals are microcrystalline, with grains similar in size to clay. As such, the Ra recoil efficiency is probably high. Our measured  $^{219}\text{Rn}$  emanation from serpentinites (Table 3) ranges from 0.22 to 1.08. Discarding the extremely high value and averaging the remaining three yields 0.23, similar to the value for basalt. We will use this value initially and compare the result to other values that could have been chosen.

Using an average  $^{238}\text{U}$  concentration of  $1.1 \mu\text{g g}^{-1}$  should produce an average of  $19 \text{ dpm kg}^{-1}$  for  $^{231}\text{Pa}$  in the 35 Ky serpentinite. Using a recoil efficiency of 0.23 in Equation 10 for the microcrystalline serpentinite grains, yields  $P = 117 \text{ atoms min}^{-1} \text{L}^{-1}$ . To convert to activity units, we multiply by  $\lambda_{223}$ . To convert this production rate to an activity of  $^{223}\text{Ra}$  we multiply by the mean life of  $^{223}\text{Ra}$  ( $1/\lambda_{223}$ ). The result is a mobile  $^{223}\text{Ra}_w$  activity of  $117 \text{ dpm L}^{-1}$ , only slightly greater than measured in the highest activity fluid sample.

The partitioning of the  $^{223}\text{Ra}$  produced between solution or adsorption can be further estimated:

$$\text{Ra}_w = \frac{P \times \text{mean life}}{(K + 1)} \quad (11)$$

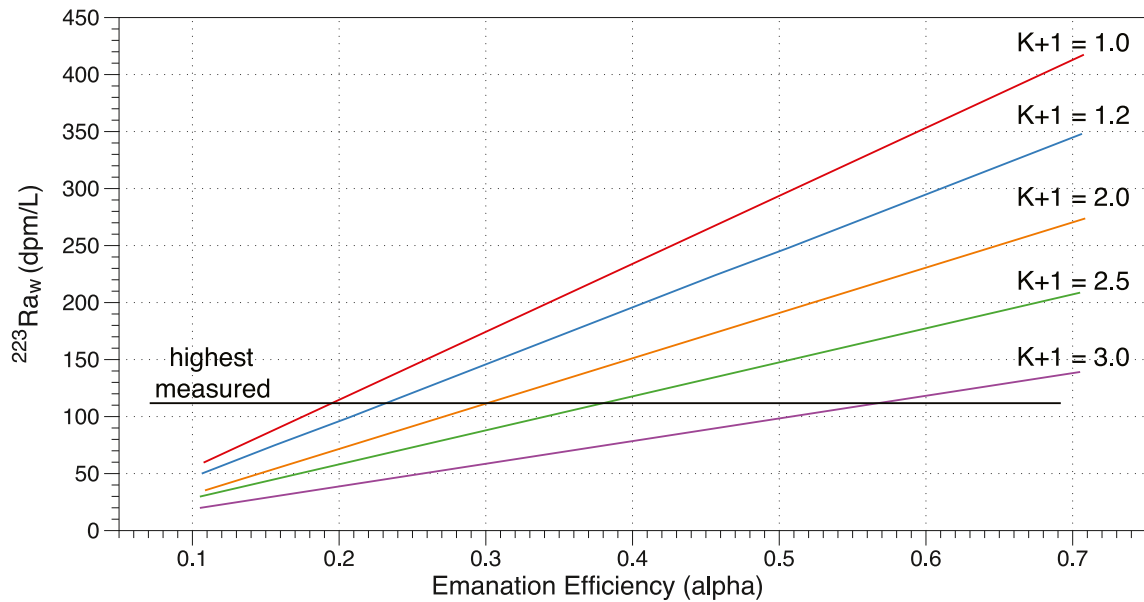


**Figure 5.** Variations in  $^{223}\text{Ra}_w$  activity in the fluids as a function of the recoil efficiency ( $\alpha$ ) for different values of adsorption, where  $R = K + 1$ . The highest measured  $^{223}\text{Ra}_w$  indicates that  $\alpha$  must be  $>0.2$  if there is no adsorption and even higher if there is adsorption.

$$K = \frac{P \times \text{mean life}}{\text{Ra}_w} - 1 = \frac{117 \text{ dpm/L}}{109 \text{ dpm/L}} - 1 = 0.08$$

Converting  $K$  to  $R$  yields  $R = 1.08$ .

Using this value in Equation 9:

$$T = \frac{1.5y}{1.08}$$

$$T = 1.4 \text{ y.}$$

It is probable that the initial  $^{223}\text{Ra}$  in the fluid was  $>109 \text{ dpm L}^{-1}$  due to decay between recoil from the rock and sample collection. The maximum limit for  $^{223}\text{Ra}$  when  $\alpha = 0.23$  is fixed by the U content of the serpentinites at  $136 \text{ dpm L}^{-1}$ . At this limit  $K = 0$ ,  $R = 1$  and:

$$T = \frac{1.5y}{1} = 1.5 \text{ y.}$$

Note that the limit for initial  $^{223}\text{Ra}_w$  is based on a recoil efficiency = 0.23. If  $\alpha$  was raised to 0.5, the mobile  $^{223}\text{Ra}$  would increase to  $254 \text{ dpm L}^{-1}$ ,  $K$  would increase to 2.3 and  $R$  to 3.3. This would decrease the fluid residence time to 0.6 y. The lower limit for  $\alpha$  is 0.21; at this value the production rate of mobile  $^{223}\text{Ra}$  is approximately equal to that measured in the fluid. Figure 5 illustrates how changes in  $\alpha$  affect  $^{223}\text{Ra}_w$  for different values of  $K$ . At the practical limit of recoil efficiency (0.7),  $K = 4$ . This low value is similar to the expected  $K$  in low pH basaltic systems; however, it was unexpected in a system with high pH. Clearly, this is a subject for additional research.

#### 4.4.3. Retardation Factor and Rock Alteration Constrained by $^{226}\text{Ra}_w$

A remaining question regards the effect rock alteration (dissolution) may have on the  $^{223}\text{Ra}_w/^{226}\text{Ra}_w$  AR. We first calculate  $^{226}\text{Ra}_w$  using Equation 10 and assuming no rock alteration or Ra precipitation from the fluid. The expected activity of  $^{230}\text{Th}$  in the 35 Ky serpentine with  $^{234}\text{U} = 950 \text{ dpm kg}^{-1}$  is  $260 \text{ dpm kg}^{-1}$ . Using 0.23 recoil efficiency for the serpentine grains, results in  $^{226}\text{Ra}$  production rate of  $1,600 \text{ atoms}^{-1} \text{ min}^{-1} \text{ L}^{-1}$  or  $1.3 \times 10^{-6} \text{ dpm min}^{-1} \text{ L}^{-1}$ . After 2 y (the maximum residence time estimated here), the available  $^{226}\text{Ra}$  activity would be  $1.4 \text{ dpm L}^{-1}$ . The average endmember  $^{226}\text{Ra}_w$  in the uncontaminated fluid samples is  $1.2 \text{ dpm L}^{-1}$ . Thus,  $K = 1.2$  and

$R = 2.2$ , well within the range of earlier estimates. Therefore, rock alteration has little effect on the  $^{223}\text{Ra}_w/^{226}\text{Ra}_w$  AR.

#### 4.4.4. Sensitivity of the Model to Porosity

Porosity strongly affects the rates of production of  $^{223}\text{Ra}$  and  $^{226}\text{Ra}$ . If the porosity of the serpentinite is higher than reported, the volume of fluid in contact with the rock would be greater. If the production rate of  $^{223}\text{Ra}$  in the rock is constant, increased fluid volume essentially dilutes the activity of mobile  $^{223}\text{Ra}$  released into solution, causing the  $^{223}\text{Ra}_w$  activity to decrease. If we increase porosity by 20% to 0.046 and keep  $\alpha = 0.23$ , the activity of mobile  $^{223}\text{Ra}$  will be 112 dpm  $\text{L}^{-1}$ , approximately our measured value. Higher porosities would yield  $^{223}\text{Ra}_w$  values below what is measured. Decreasing porosity by 50% to 0.019 and keeping  $\alpha = 0.23$  increases the activity of mobile  $^{223}\text{Ra}$  to 272 dpm  $\text{L}^{-1}$ . This would cause  $R$  to increase to 2.5 (i.e., 272/109). Using this value for  $R$  in Equation 9 results in an even lower residence time of 0.6 y. We conclude that even if porosity has been substantially under- or over-estimated, the changes to  $R$  and  $T$  are minor.

#### 4.5. High $^{228}\text{Th}$ and $^{226}\text{Ra}$ in One Sample

The Calypso fluid sample (J2-1108-Chem7) was unusual in that it had substantially higher  $^{228}\text{Th}_w$  (0.82 dpm  $\text{L}^{-1}$ ) and  $^{226}\text{Ra}_w$  (2.5 dpm  $\text{L}^{-1}$ ) activity than the other samples ( $^{228}\text{Th}_w$ : 0.08–0.35 dpm  $\text{L}^{-1}$ ;  $^{226}\text{Ra}_w$ : 0.9–1.4 dpm  $\text{L}^{-1}$ ). These are not corrected for entrainment of seawater using  $\text{Mg}^{2+}$ . The Calypso sample also had a low volume (0.100 L) and contained abundant fine particles. It is possible that dissolution of some of these particles could explain the high observed activities. Actively venting carbonate chimney samples had  $^{226}\text{Ra}_f$  activities in the range 66–1,700 dpm  $\text{kg}^{-1}$  (Table S1) but undetectable  $^{228}\text{Th}$  (even though the detection level is lower than for  $^{226}\text{Ra}$ ). If the particles were near the upper range of our measurements, dissolution of at least 0.4 g of carbonate is required to account for the  $^{226}\text{Ra}$  fluid activity. But this could not simultaneously account for the high measured  $^{228}\text{Th}$ . The Calypso vent had the lowest maximum temperature of all samples measured (32.9°C). We speculate that this sample likely represents a high fraction of water that became isolated from the primary flow field for an extended period of time, possibly leading to some rock dissolution (see Section 4.6) and continued input of  $^{223}\text{Ra}$  by alpha recoil. The high  $^{228}\text{Th}$  activity remains a mystery.

#### 4.6. Activities of $^{226}\text{Ra}$ in Serpentinite

Once released to solution radium may be sequestered by adsorption or by uptake into accessory minerals. We have shown that adsorption is very low in the serpentinites (Sections 4.4.2 and 4.4.3), yet measurements of  $^{226}\text{Ra}$  in the bulk serpentinites (Table S1) ranged in value from <60 to 1,075 dpm  $\text{kg}^{-1}$ ; in some cases, the  $^{226}\text{Ra}$  activity exceeded the  $^{238}\text{U}$  activity. With  $K$  being so low, this implies some  $^{226}\text{Ra}$  must be incorporated into accessory minerals within the serpentinites. Besides Mg, other alkaline metal concentrations of bulk Lost City serpentinites are also quite variable, with Ba ranging from below detection to 17 mg  $\text{kg}^{-1}$  (Rouméjon et al., 2018) and Sr ranging from 3 to 760 mg  $\text{kg}^{-1}$  (Früh-Green et al., 2018). Accessory minerals with high Ba or Sr concentrations probably also sequester Ra; possible candidates for incorporating Ra are barite, calcite, celestite, and brucite.

Although sulphate is depleted in the fluids, concentrations remain in the range 1–4 mmol  $\text{kg}^{-1}$  (Kelley et al., 2005; Lang et al., 2012; Seyfried et al., 2015). Thus, Ba released from the rocks could precipitate as  $\text{BaSO}_4$ . At high pH  $\text{CO}_3^{2-}$  is the primary carbonate species in the fluids and may cause Ba and Ra to coprecipitate with  $\text{CaCO}_3$ . Addition of carbonate ions to sea water to produce  $\text{CaCO}_3$  is a standard separation mechanism for removing Ba and Ra from seawater samples for further analysis (Foster et al., 2004). Likewise, Sr could precipitate as celestite and carry Ba and Ra. Brucite is a common mineral associated with the serpentinites (Bach et al., 2004; Früh-Green et al., 2004; Klein et al., 2013). We are not aware of studies of Ba in brucite from Lost City, but Pokrovsky and Schott (2004) reported that a sample of brucite from Cedar Hill, PA, contained 77 mg  $\text{kg}^{-1}$  Ba. There could be other minerals that contain Ba and Ra enrichments that we have not considered. Finding significant activities of  $^{226}\text{Ra}$  in some serpentinites indicates accessory minerals enriched in Ba and/or Sr are likely present.

The sequestering of Ra in such minerals will be much more important for  $^{226}\text{Ra}$  than for  $^{223}\text{Ra}$ , because  $^{226}\text{Ra}$  will remain in stable minerals for several thousand years, while  $^{223}\text{Ra}$  completely decays within 2 months. The close agreement between the predicted and measured  $^{226}\text{Ra}$  activity in the fluids (Section 4.4.3) indicates that this process is not important on a time scale of a few years; instead, it is a cumulative effect that slowly enriches

**Table 4**  
*Compilation of Residence Times and Radium Activities ( $\text{dpm L}^{-1}$ ) From Hydrothermal Systems*

Location	System type	Fluid temp. ( $^{\circ}\text{C}$ )	$^{223}\text{Ra}$	$^{226}\text{Ra}$	$^{228}\text{Ra}$	Fluid residence time (yrs)
Reykjanes Peninsula, Iceland [1]	Continental geothermal wells	240–295	0.1–1.0	6.0–26	11–26	1–5
Balaruc-les-Bains, France [2]	Continental hot spring	50	0.6–4.9	21–51	10–30	--
Yellowstone, USA [3]	Continental hot spring	45–92	0.0001–3	0.04–1.0	0.05–21	--
Axial JDFR [4]	Mafic hydrothermal	240	--	11–29	15	--
South Cleft, JDFR [4]	Mafic hydrothermal	30–286	--	40–45	42	$\leq 2$
North Cleft, JDFR [4]	Mafic hydrothermal	286–310	--	66–81	38–46	2–4
Main Endeavor Field, JDFR [5]	Mafic hydrothermal	245–370	--	2.4–24	39–63	$<3$
Main Endeavor Field, JDFR [6]	Mafic hydrothermal	75–340	0.8–1.9	2–28	4–25	--
High Rise Field, JDFR [6]	Mafic hydrothermal	322–337	--	8–47	2–31	--
Baby Bare and IODP Hole 1026B, JDFR [6]	Ridge flank, 3.5 My crust	18–63	0.008–0.11	0.2–0.4	0.02–0.04	--
Brothers Volcano, Kermadec Arc [7]	Intraoceanic arc	$<150$	Bdl – 0.63	0.1–2.4	Bdl – 5.4	--
Brothers Volcano, Kermadec Arc [7]	Intraoceanic arc	170–311	0.1–1.6	1.7–11	2–25	--
Puna Ridge, Hawaii [8]	Hot spot volcanic chain	2.5–4	0.019	0.22	0.008	--
Lost City Hydrothermal Field [9]	Ultramafic hydrothermal	32–95	13–109	0.8–5.9	Bdl	$<2$

*Note.* JDFR is Juan de Fuca Ridge. Data compiled from 1: Kadko et al. (2007); 2: Condomines et al. (2012); 3: Moloney et al. (2011); 4: Kadko and Butterfield (1998) (Mg  $<10$  mM); 5: Kadko and Moore (1988); 6: Kipp et al. (2018); 7: Neuholz et al. (2020); 8: Moore et al. (2008); 9: this work.

$^{226}\text{Ra}$  over its mean life of 2,500 y. The presence of substantial activities of solid phase  $^{226}\text{Ra}$  in the serpentinites provides a potential source of  $^{226}\text{Ra}$  to the fluids if conditions change in such a way as to dissolve the accessory mineral (see Section 4.5).

#### 4.7. Comparison With Residence Times From Other Systems, and Implications for Organic Synthesis and Stability

The flow paths of water in ultramafic hydrothermal systems have the potential to differ significantly from those hosted on mafic rocks. The extensive faulting and fracturing that occurs in ultramafic settings could cause fluids to be sequestered in the subseafloor for longer periods of time or create more meandering flow paths. The subseafloor temperatures at Lost City ( $\sim 180^{\circ}\text{C}$ , Seyfried et al., 2015) are also cooler than most focused flow from mafic systems ( $>300^{\circ}\text{C}$ , German & Von Damm, 2004), providing less of a thermal drive for fluid convection. It is therefore somewhat surprising that the residence time of Lost City fluids is similar to the  $<3$  y that is observed at neovolcanic fields hosting  $>350^{\circ}\text{C}$  black smoker fluids (Kadko & Butterfield, 1998; Kadko & Moore, 1988). Table 4 is a summary of Ra measurements and fluid residence times for a variety of hydrothermal systems.

These relatively short residence times have implications for the extent to which sluggish geochemical reactions will proceed. The high concentrations of methane in Lost City fluids have been interpreted to result from abiotic synthesis (Proskurowski et al., 2008), despite such reactions requiring temperatures  $>350^{\circ}\text{C}$  to overcome kinetic inhibitions (McCollom & Seewald, 2007). Recently, clumped isotope analysis of methane from Lost City fluids indicated that it formed at temperatures higher than those present in the modern-day subseafloor (Wang et al., 2018). The current interpretation is that methane—formed at an earlier time period when temperatures of the system were hotter—is stored over millennia and is now being stripped from the rocks into modern fluids (Kelley & Fruh-Green, 2001; Klein et al., 2020; McDermott et al., 2020; Wang et al., 2018). The short residence times observed at Lost City support this interpretation, as fluids would not be in the subseafloor for a long enough time to allow the kinetic inhibition for abiotic methane formation to be overcome.

The presence and stability of non-volatile organic molecules have been of particular interest at Lost City as the high  $\text{H}_2$  concentrations have the potential to produce them abiotically (McCollom & Seewald, 2007). Abiotic formate is present in micro-molar concentrations in the Lost City fluids (Lang et al., 2010, 2018), and the amino acid tryptophan has been reported in drill cores from the Atlantis Massif (Ménez et al., 2018).

After their formation, the presence of these organic molecules and possibly others may lead to and support the development of a biotic system (Martin & Russell, 2007).

The decomposition rates of amino acids at temperatures similar to the seafloor of Lost City have been estimated using mineral-buffered and mineral-free experiments (McCollom, 2013). The resulting half-lives indicate that alky- $\alpha$ -amino acids could survive a transport time of several years so long as temperatures remain below  $\sim 140^{\circ}\text{C}$  but would be destroyed if temperatures reach  $\sim 180^{\circ}\text{C}$ , though these values would shift based on exposed surface and types of mineral assemblages (McCollom, 2013). Therefore, at the residence times reported here, compounds formed in the ultramafic recesses of the Atlantis Massif could indeed be accumulated and exported out of the system without being destroyed.

#### 4.8. Implications of Elevated $^{223}\text{Ra}$ for Detecting Ultramafic Fluid Flow

The mechanisms that lead to extraordinarily high  $^{223}\text{Ra}$  in Lost City fluids are likely ubiquitous in ultramafic systems, as they are the direct result of the hydration of peridotite accompanied by uranium enrichment over long periods of time. Elevated  $^{223}\text{Ra}$  activities have also been observed in the mixed ultramafic-mafic Von Damm Vent Field (Frankle et al., 2020), suggesting that this signature may indeed be prevalent in ultramafic systems more generally.

If correct, there is the potential to exploit this feature to identify as yet undiscovered ultramafic-influenced hydrothermal venting. The number of such systems that have been studied is small because fluids from serpentinite-hosted fields cannot easily be identified by traditional water-column anomalies (Larson et al., 2015). The fluids often have a lower metal content and so do not create the particle signatures that can be detected in transmissivity anomalies. The fluids are also frequently lower temperature than mafic systems and so cause smaller temperature deviations in the water column. Since  $^{223}\text{Ra}$  is both relatively short-lived (11.4-day half-life) and does not reach these very high activities in mafic hydrothermal systems or sediments (Kipp et al., 2018; Neuholz et al., 2020), its presence could be a strong indication of local input of ultramafic fluids.

In 2011, elevated  $^{223}\text{Ra}$  activities that were decoupled from other Ra isotope sources were observed in the water column near the Trans-Atlantic Geotraverse (TAG;  $26^{\circ}\text{N}$ , Mid-Atlantic Ridge) hydrothermal field as part of a US GEOTRACES transect across the Atlantic Ocean (Charette et al., 2015). The highest  $^{223}\text{Ra}$  activities occurred in the deepest seawater, well below the neutrally buoyant plume. The signature was attributed to decay of actinium-227 that is elevated in the plume and could be scavenged by particles that fall out of the plume (Kipp et al., 2015). Given what we now know about elevated  $^{223}\text{Ra}$  in ultramafic fluids, a second intriguing possibility is that there are low levels of ultramafic-influenced hydrothermal fluid input in the region near the TAG field. Ultramafic rocks are a common feature along the slow-spreading Mid-Atlantic Ridge and, while the fluids from TAG are consistent with a mafic host rock (Campbell et al., 1988), the field sits atop the hanging wall of an active detachment fault (Tivey et al., 2003). Low-temperature venting occurs in a region named Shimmering Mounds to the north of the field that is associated with the detachment surface (Szitkar et al., 2019). These regions are potentially associated with ultramafic rocks and serpentinization (Zonenshain et al., 1989) and could therefore be a source of  $^{223}\text{Ra}$  into the water column.

## 5. Conclusions

At the Lost City Hydrothermal Field, unusually high  $^{223}\text{Ra}$  activities were measured for a hydrothermal system. We attribute this to the age of the system and the U enrichment in the serpentinite subsurface. Using the radiochemistry of the hydrothermal fluids and solids as constraints, residence times of fluids passing through the system were determined to be less than 2 y. The upper limit of this residence time is insensitive to recoil efficiency, porosity, and the parent content of the serpentinite. These data also require  $R$  (the retardation of the movement of radium compared to the fluids) to have low values, between 1 and 4. Rock alteration has little effect on the  $^{223}\text{Ra}_w/^{226}\text{Ra}_w$  AR.

This residence time is remarkably similar to that of basalt-hosted axial hydrothermal systems. The similarity may be due in part to the hydrological behaviors of the systems, with buoyant fluids supplying the focused flow of hydrothermal vent fields channeled primarily through faults and fractures (Lowell, 2017; Titarenko & McCaig, 2016). These relatively short timescales of fluids in the crust may limit the extent to which chemical

reactions with slower kinetics, such as abiotic methane formation, can proceed. If similarly high  $^{223}\text{Ra}$  activities are common in ultramafic-hosted hydrothermal fluids, this signature could be used to identify new fields or to track water masses and mixing processes near the seabed.

## Data Availability Statement

All data used in this article have been submitted to the database <https://www.bco-dmo.org/project/658604>.

## Acknowledgments

The authors thank the captain and crew of the R/V *Atlantis* and the R.S.S. *James Cook* and the expedition leaders and crews of the ROV *Jason II* as well as the IODP Expedition 357 project managers and the MeBo and RD2 seabed rock drill teams. Funding was provided by NSF-OCE grants 1536702 to SQL and 1736321 to WSM; funding for Expedition 357 was provided by the European Consortium for Ocean Research Drilling (ECORD). The authors also acknowledge financial support from the Deep Carbon Observatory and the Swiss National Science Foundation grant 200021\_163187. The authors thank David Butterfield (PMEL) for providing the concentrations of magnesium in the fluids. Analytical support was provided by Michael Bizimis and Jim Sexton at the University of South Carolina Center for Elemental Mass Spectrometry Analysis.

## References

- Allen, D. E., & Seyfried, W. E. (2004). Serpentinization and heat generation: Constraints from Lost City and rainbow hydrothermal systems. *Geochimica et Cosmochimica Acta*, 68(6), 1347–1354.
- Bach, W., Garrido, C. J., Paulick, H., Harvey, J., & Rosner, M. (2004). Seawater-peridotite interactions: First insights from ODP Leg 209, MAR 15°N. *Geochimica et Cosmochimica Acta*, 5, Q09F26.
- Bayrakci, G., Falcon-Suarez, I. H., Minshull, T. A., North, L., Barker, A., Zihlmann, B., et al. (2018). Anisotropic physical properties of mafic and ultramafic rocks from an oceanic core complex. *Geochemistry, Geophysics, Geosystems*, 19, 4366–4384.
- Bemis, K., Lowell, R. P., & Farough, A. (2012). Diffuse flow on and around hydrothermal vents at mid-ocean ridges. *Oceanography* 25(1): 182–191.
- Bethke, C. M., & Johnson, T. M. (2002). Paradox of groundwater age. *Geology*, 30(2), 107–110.
- Boschi, C., Früh-Green, G. L., Delacour, A., Karson, J. A., & Kelley, D. S. (2006). Mass transfer and fluid flow during detachment faulting and development of an oceanic core complex, Atlantis Massif (MAR 30°N). *Geochemistry, Geophysics, Geosystems*, 7, Q01004.
- Cai, P., Shi, X., Moore, W. S., & Dai, M. (2012). Measurement of  $^{224}\text{Ra}$ : $^{228}\text{Th}$  disequilibrium in coastal sediments using a delayed coincidence counter. *Marine Chemistry*, 138–139, 1–6. <https://doi.org/10.1016/j.marchem.2012.05.004>
- Campbell, A. C., Palmer, M. R., Klinkhammer, G. P., Bowers, T. S., Edmond, J. M., Lawrence, J. R., et al. (1988). Chemistry of hot springs on the Mid-Atlantic Ridge. *Nature* 335, 514–519.
- Cann, J. R., Blackman, D. K., Smith, D. K., McAllister, E., Janssen, B., Mello, S., et al. (1997). Corrugated slip surfaces formed at ridge-transform intersections on the Mid-Atlantic Ridge. *Nature*, 385(6614), 329–332.
- Charette, M. A., Morris, P. J., Henderson, P. B., & Moore, W. S. (2015). Radium isotope distributions during the US GEOTRACES North Atlantic cruises. *Marine Chemistry*, 177, 184–195.
- Chen, J. H., Edwards, R. L., & Wasserburg, G. J. (1986). U-238, U-234, and Th-232 in seawater. *Earth and Planetary Science Letters*, 80(3–4), 241–251.
- Cochran, J. K., & Kadko, D. C. (2008). Uranium and thorium series radionuclides in groundwaters. In S. Krishnaswami & J. K. Cochran (Eds.), *U-Th series nuclides in aquatic systems* (Vol. 13, pp. 345–382). Elsevier Science Bv.
- Condomines, M., Gourdin, E., Gataniou, D., & Seidel, J. L. (2012). Geochemical behavior of radium isotopes and radon in a coastal thermal system (Balaruc-les-Bains, South of France). *Geochimica et Cosmochimica Acta*, 98, 160–176.
- Firestone, R. B. (1999). In C. M. Baglin & S. Y. F. Chu (Eds.), *Table of isotopes* (8 ed.). Wiley.
- Fisher, A. T. (2004). Rates and patterns of fluid circulation. In E. E. Davis & E. Elderfield (Eds.), *Hydrogeology of the oceanic lithosphere* (pp. 151–188). Cambridge University Press.
- Fisher, A. T., Davis, E. E., Hutnak, M., Spiess, V., Zuhlsdorff, L., Cherkaoui, A., et al. (2003). Hydrothermal recharge and discharge across 50 km guided by seamounts on a young ridge flank. *Nature*, 421(6923), 618–621.
- Foster, D. A., Staubwasser, M., & Henderson, G. M. (2004).  $^{226}\text{Ra}$  and Ba concentrations in the Ross Sea measured with multicollector ICP mass spectrometry. *Marine Chemistry*, 87, 59–71.
- Frankle, J., Moore, W. S., Benitez-Nelson, C. R., & Lang, S. Q. (2020). Remarkably elevated activity of short-lived radium in an ultramafic hydrothermal system on the Mid-Cayman Rise. AGU. Abstract H213-03 presented at 2020 Fall Meeting.
- Früh-Green, G. L., Connolly, J. A. D., Kelley, D. S., Plas, A., & Grobóty, B. (2004). Serpentinization of oceanic peridotites: Implications for geochemical cycles and biological activity. In W. D. Wilcock, D. S. Kelley, E. DeLong, & C. Cary (Eds.), *The seafloor biosphere at mid-ocean ridges*, AGU Geophysical Monograph (Vol. 144, pp. 119–136).
- Früh-Green, G. L., Kelley, D. S., Bernasconi, S. M., Karson, J. A., Ludwig, K. A., Butterfield, D. A., et al. (2003). 30,000 y of hydrothermal activity at the Lost City vent field. *Science*, 301(5632), 495–498.
- Früh-Green, G. L., Orcutt, B. N., Rouméjon, S., Lilley, M. D., Morono, Y., Cotterill, C., et al. (2018). Magmatism, serpentinization and life: Insights through drilling the Atlantis Massif (IODP Expedition 357). *Lithos*, 323, 137–155.
- German, C. R., & Von Damm, K. L. (2004). Hydrothermal processes. In H. D. Holland, K. K. Turekian, & H. Elderfield (Eds.), *Treatise on Geochemistry* (Vol. 6, pp. 181–222). Elsevier-Pergamon Oxford.
- Godard, M., Awaji, S., Hansen, H., Hellebrand, E., Brunelli, D., Johnson, K., et al. (2009). Geochemistry of a long in situ section of intrusive slow-spread oceanic lithosphere: Results from IODP Site U1309 (Atlantis Massif, 30°N Mid-Atlantic-Ridge). *Earth and Planetary Science Letters*, 279(1–2), 110–122.
- Hammond, D. E., Zuckin, J. G., & Ku, T. L. (1988). The kinetics of radioisotope exchange between brine and rock in a geothermal system. *Journal of Geophysical Research*, 93(B11), 13175–13186.
- Kadko, D. (1996). Radioisotopic studies of submarine hydrothermal vents. *Reviews of Geophysics*, 34(3), 349–366.
- Kadko, D., & Butterfield, D. A. (1998). The relationship of hydrothermal fluid composition and crustal residence time to maturity of vent fields on the Juan de Fuca Ridge. *Geochimica et Cosmochimica Acta*, 62(9), 1521–1533.
- Kadko, D., Gronvold, K., & Butterfield, D. (2007). Application of radium isotopes to determine crustal residence times of hydrothermal fluids from two sites on the Reykjanes Peninsula, Iceland. *Geochimica et Cosmochimica Acta*, 71(24), 6019–6029.
- Kadko, D., Koski, R., Tatsumoto, M., & Bouse, R. (1985/1986). An estimate of hydrothermal fluid residence times and vent chemistry growth-rates based on Pb-210-Pb ratios and mineralogic studies of sulfides dredged from the Juan de Fuca Ridge. *Earth and Planetary Science Letters*, 76(1–2), 35–44.
- Kadko, D., & Moore, W. S. (1988). Radiochemical constraints on the crustal residence time of submarine hydrothermal fluids—Endeavor Ridge. *Geochimica et Cosmochimica Acta*, 52(3), 659–668.



- Karson, J. A., Früh-Green, G. L., Kelley, D. S., Williams, E. A., Yoerger, D. R., & Jakuba, M. (2006). Detachment shear zone of the Atlantis Massif core complex, Mid-Atlantic Ridge, 30°N. *Geochemistry, Geophysics, Geosystems*, 7(6), Q06016.
- Kelley, D. S., & Früh-Green, G. L. (2001). Volatile lines of descent in submarine plutonic environments: Insights from stable isotope and fluid inclusion analyses. *Geochimica et Cosmochimica Acta*, 65, 3325–3346.
- Kelley, D. S., Karson, J. A., Blackman, D. K., Früh-Green, G. L., Butterfield, D. A., Lilley, M. D., et al. (2001). An off-axis hydrothermal vent field near the Mid-Atlantic Ridge at 30°N. *Nature*, 412(6843), 145–149.
- Kelley, D. S., Karson, J. A., Früh-Green, G. L., Yoerger, D. R., Shank, T. M., Butterfield, D. A., et al. (2005). A serpentinite-hosted ecosystem: The Lost City Hydrothermal Field. *Science*, 307(5714), 1428–1434.
- Kipp, L., Charette, M., Hammond, D., & Moore, W. S. (2015). Hydrothermal vents: A previously unrecognized source of actinium-227 to the deep ocean. *Marine Chemistry*, 177, 583–590.
- Kipp, L. E., Sanial, V., Henderson, P. B., van Beek, P., Reyss, J. L., Hammond, D. E., et al. (2018). Radium isotopes as tracers of hydrothermal inputs and neutrally buoyant plume dynamics in the deep ocean. *Marine Chemistry*, 201, 51–65.
- Kiro, Y., Yecheili, Y., Voss, C. I., Starinsky, A., & Weinstein, Y. (2012). Modeling radium distribution in coastal aquifers during sea level changes: The Dead Sea case. *Geochimica et Cosmochimica Acta*, 88, 237–254.
- Kiro, Y., Weinstein, Y., Starinsky, A., & Yecheili, Y. (2013). Groundwater ages and reaction rates during seawater circulation in the Dead Sea aquifer. *Geochimica et Cosmochimica Acta*, 122, 17–35.
- Klein, F., Grozeva, N. G., & Seewald, J. S. (2019). Abiotic methane synthesis and serpentinization in olivine-hosted fluid inclusions. *Proceedings of the National Academy of Sciences of the United States of America*, 116, 17666–17672.
- Klein, F., Wolfgang Bach, W., Thomas, M., & McCollom, T. M. (2013). Compositional controls on hydrogen generation during serpentinization of ultramafic rocks. *Lithos*, 178, 55–69. <https://doi.org/10.1016/j.lithos.2013.03.008>
- Krishnaswami, S., Graustein, W. C., Turekian, K. K., & Dowd, J. F. (1982). Radium, thorium and radioactive lead isotopes in groundwaters—Application to the in situ determination of adsorption-desorption rate constants and retardation factors. *Water Resources Research*, 18(6), 1663–1675.
- Lang, S. Q., & Benitez-Nelson, B. (2021). Hydrothermal Organic Geochemistry (HOG) sampler for deployment on deep-sea submersibles. *Deep Sea Research Part I: Oceanographic Research Papers*, 173, 103529.
- Lang, S. Q., Butterfield, D. A., Schulte, M. S., Kelley, D. S., & Lilley, M. D. (2010). Elevated concentrations of formate, acetate, and dissolved organic carbon found at the Lost City Hydrothermal Field. *Geochimica et Cosmochimica Acta*, 74, 941–952.
- Lang, S. Q., Früh-Green, G. L., Bernasconi, S. M., Brazelton, W. J., Schrenk, M. O., & McGonigle, J. M. (2018). Deeply-sourced formate fuels sulfate reducers but not methanogens at Lost City Hydrothermal Field. *Scientific Reports*, 8, 755.
- Lang, S. Q., Früh-Green, G. L., Bernasconi, S. M., Lilley, M. D., Proskurowski, G., Méhay, S., & Butterfield, D. A. (2012). Microbial utilization of abiogenic carbon and hydrogen in a serpentinite-hosted system. *Geochimica et Cosmochimica Acta*, 92, 82–99.
- Lang, S. Q., Lilley, M. D., Baumberger, T., Früh-Green, G. L., Walker, S. L., Brazelton, W. J., et al. (2021). Extensive decentralized hydrogen export from the Atlantis Massif. *Geology*.
- Larson, B. I., Lang, S. Q., Lilley, M. D., Olson, E. J., Lupton, J., Nakamura, K., & Buck, N. (2015). Stealth export of hydrogen and methane from a low-temperature serpentinization system. *Deep-Sea Research Part II: Topical Studies in Oceanography*, 121, 233–245. <https://doi.org/10.1016/j.dsr2.2015.05.007>
- Lowell, R. P. (2017). A fault-driven circulation model for the Lost City Hydrothermal Field. *Geophysical Research Letters*, 44, 2703–2709.
- Ludwig, K. A., Shen, C. C., Kelley, D. S., Cheng, H., & Edwards, R. L. (2011). U-Th systematics and Th-230 ages of carbonate chimneys at the Lost City Hydrothermal Field. *Geochimica et Cosmochimica Acta*, 75(7), 1869–1888.
- Maiti, K., Charette, M. A., Buesseler, K. O., Zhou, K. B., Henderson, P., Moore, W. S., et al. (2015). Determination of particulate and dissolved Th-228 in seawater using a delayed coincidence counter. *Marine Chemistry*, 177, 196–202.
- Martin, W., & Russell, M. J. (2007). On the origin of biochemistry at an alkaline hydrothermal vent. *Philosophical Transactions of the Royal Society B*, 362(1486), 1887–1925.
- McCaig, A., Covey-Crump, S. J., Ben Ismail, W., & Lloyd, G. E. (2007). Fast diffusion along mobile grain boundaries in calcite. *Contributions to Mineralogy and Petrology*, 153(2), 159–175.
- McCollom, T. M. (2013). The influence of minerals on decomposition of the *n*-alkyl- $\alpha$ -amino acid norvaline under hydrothermal conditions. *Geochimica et Cosmochimica Acta*, 104, 330–357.
- McCollom, T. M., & Seewald, J. S. (2007). Abiotic synthesis of organic compounds in deep-sea hydrothermal environments. *Chemical Reviews*, 107(2), 382–401.
- McDermott, J. M., Sylva, S. P., Ono, S., German, C. R., & Seewald, J. S. (2020). Abiotic redox reactions in hydrothermal mixing zones: Decreased energy availability for the subsurface biosphere. *Proceedings of the National Academy of Sciences of the United States of America*, 117(34), 20453–20461.
- Menéz, B., Pisapia, C., Andreani, M., Jamme, F., Vanbellingen, Q. P., Brunelle, A., et al. (2018). Abiotic synthesis of amino acids in the recesses of the oceanic lithosphere. *Nature*, 564, 59–63.
- Michard, A., & Albarede, F. (1985). Hydrothermal uranium uptake at ridge crests. *Nature*, 317(6034), 244–246.
- Moloney, T. P., Sims, K. W., & Kaszuba, J. P. (2011). Uranium and Thorium decay series isotopic constraints on the source and residence time of solutes in the yellowstone hydrothermal system. *University of Wyoming-National Park Service Research Center*, 33, 187–207.
- Moore, W. S. (1976). Sampling Ra-228 in the deep ocean. *Deep-Sea Research*, 23(7), 647–651.
- Moore, W. S. (1984). Radium isotope measurements using germanium detectors. *Nuclear Instruments and Methods in Physics Research*, 223(2–3), 407–411.
- Moore, W. S. (2008). Fifteen years experience in measuring Ra-224 and Ra-223 by delayed-coincidence counting. *Marine Chemistry*, 109(3–4), 188–197.
- Moore, W. S., & Sackett, W. M. (1964). Uranium and Thorium series disequilibrium in sea water. *Journal of Geophysical Research*, 69, 5401–5405.
- Moore, W. S., & Arnold, R. (1996). Measurement of Ra-223 and Ra-224 in coastal waters using a delayed coincidence counter. *Journal of Geophysical Research*, 101(C1), 1321–1329.
- Moore, W. S., & Cai, P. H. (2013). Calibration of RaDeCC systems for Ra-223 measurements. *Marine Chemistry*, 156, 130–137.
- Moore, W. S., Ussler, W., & Paull, C. K. (2008). Short-lived radium isotopes in the Hawaiian margin: Evidence for large fluid fluxes through the Puna Ridge. *Marine Chemistry*, 109(3–4), 421–430.
- Mottl, M. J., Wheat, G., Baker, E., Becker, N., Davis, E., Feely, R., et al. (1998). Warm springs discovered on 3.5 Ma oceanic crust, eastern flank of the Juan de Fuca Ridge. *Geology*, 26(1), 51–54.

- Neira, N. M., Clark, J. F., Fisher, A. T., Wheat, C. G., Haymon, R. M., & Becker, K. (2016). Cross-hole tracer experiment reveals rapid fluid flow and low effective porosity in the upper oceanic crust. *Earth and Planetary Science Letters*, *450*, 355–365.
- Neuholz, R., Schnetger, B., Kleint, C., Koschinsky, A., Lettmann, K., Sander, S., et al. (2020). Near-field hydrothermal plume dynamics at Brothers Volcano (Kermadec Arc): A short-lived radium isotope study. *Chemical Geology*, *533*, 119379.
- Phillips, G. W., & Marlow, K. W. (1976). Automatic analysis of gamma-ray spectra from germanium detectors. *Nuclear Instruments and Methods*, *137*, 525.
- Pokrovsky, O. S., & Schott, J. (2004). Experimental study of brucite dissolution and precipitation in aqueous solutions: Surface speciation and chemical affinity control. *Geochimica et Cosmochimica Acta*, *68*, 31–45.
- Proskurowski, G., Lilley, M. D., Seewald, J. S., Früh-Green, G. L., Olson, E. J., Lupton, J. E., et al. (2008). Abiogenic hydrocarbon production at Lost City Hydrothermal Field. *Science*, *319*(5863), 604–607.
- Rajaomahefasoa, R. E., Voltaggio, M., Rakotomandrindra, P. F., Ratsimbazafy, J. B., Spadoni, M., & Rakoto, H. A. (2019). Radium isotopes for groundwater age and sustainability in the highland Antananarivo, Madagascar. *Journal of African Earth Sciences*, *156*, 94–107.
- Rama, & Moore, W. S. (1990). Submicronic porosity in common minerals and emanation of radon. *Nuclear Geophysics*, *4*, 467–473.
- Roumèjon, S., Früh-Green, G. L., Orcutt, B. N., & the IODP Expedition 357 Science Party. (2018). Alteration heterogeneities in peridotites exhumed on the southern wall of the Atlantis Massif (IODP Expedition 357). *Journal of Petrology*, *59*, 1329–1358. <https://doi.org/10.1093/ptrology/egy065>
- Seitz, M. G., & Hart, S. R. (1973). Uranium and boron distributions in some oceanic ultramafic rocks. *Earth and Planetary Science Letters*, *21*(1), 97–107.
- Seyfried, W. E., Jr, Pester, N. J., Tutolo, B. M., & Ding, K. (2015). The Lost City Hydrothermal System: Constraints imposed by vent fluid chemistry and reaction path models on seafloor heat and mass transfer processes. *Geochimica et Cosmochimica Acta*, *163*, 59–79.
- Sojo, V., Herschy, B., Whicher, A., Camprubi, E., & Lane, N. (2016). The origin of life in alkaline hydrothermal vents. *Astrobiology*, *16*(2), 181–197.
- Szitar, F., Dymant, J., Petersen, S., Bialas, J., Klischies, M., Graber, S., et al. (2019). Detachment tectonics at Mid-Atlantic Ridge 26°N. *Scientific Reports*, *9*, 11830.
- Titarenko, S. S., & McCaig, A. M. (2016). Modelling the Lost City Hydrothermal Field: Influence of topography and permeability structure. *Geofluids*, *16*, 314–328.
- Tivey, M. A., Schouten, K., & Kleinrock, M. C. (2003). A near-bottom magnetic survey of the Mid-Atlantic Ridge axis at 26°N: Implications for the tectonic evolution of the TAG segment. *Journal of Geophysical Research*, *108*(B5), 227.
- Tutolo, B. M., Mildner, D. F. R., Gagnon, C. V. L., Saar, M. O., & Seyfried, W. E., Jr. (2016). Nanoscale constraints on porosity generation and fluid flow during serpentinization. *Geology*, *44* (2), 103–106.
- Van Der Loeff, M. M. R., & Moore, W. S. (1999). In K. Grasshoff, K. Kremling, & M. Ehrhardt (Eds.), *Determination of natural radioactive tracers in methods of seawater analysis* (3rd ed., pp. 365–398). Wiley-VCH Publishers.
- Von Damm, K. L., Edmond, J. M., Grant, B., & Measures, C. I. (1985). Chemistry of submarine hydrothermal solutions at 21°N, East Pacific Rise. *Geochimica et Cosmochimica Acta*, *49*(11), 2197–2220.
- Von Damm, K. L., & Lilley, M. D. (2004). Diffuse flow hydrothermal fluids from 9°50'N East Pacific Rise: Origin, evolution and biogeochemical controls. *Subseafloor Biosphere at Mid-Ocean Ranges*, *144*, 245–268.
- Wang, D. T., Reeves, E. P., McDermott, J. M., Seewald, J. S., & Ono, S. (2018). Clumped isotopologue constraints on the origin of methane at seafloor hot springs. *Geochimica et Cosmochimica Acta*, *223*, 141–158.
- Wankel, S. D., Germanovich, L. N., Lilley, M. D., Genc, G., DiPerna, C. J., Bradley, A. S., et al. (2011). Influence of subsurface biosphere on geochemical fluxes from diffuse hydrothermal fluids. *Nature Geoscience*, *4*(7), 461–468.
- Weinstein, Y., Friedheim, O., Odintsov, L., Harlavan, Y., Nuriel, P., Lazar, B., & Burg, A. (2021). Using radium isotopes to constrain the age of saline groundwater, implications to seawater intrusion in aquifers. *Journal of Hydrology*, *598*, 126412.
- Wheat, C. G., Elderfield, H., Mottl, M. J., & Monnins, C. (2000). Chemical composition of basement fluids within an oceanic ridge flank: Implications for along-strike and across-strike hydrothermal circulation. *Journal of Geophysical Research*, *105*(B6), 13437–13447.
- Zonenshain, L. P., Kuzmin, M. I., Lisitsin, A. P., Bogdanov, Y. A., & Baranov, B. V. (1989). Tectonics of the Mid-Atlantic rift valley between the TAG and MARK areas (26°–24°N): Evidence for vertical tectonism. *Tectonophysics* *159*, 1–23.

## References From the Supporting Information

- Butterfield, D. A., & Massoth, G. J. (1994). Geochemistry of North Cleft segment vent fluids—Temporal changes in chlorinity and their possible relation to recent volcanism. *Journal of Geophysical Research*, *99*(B3), 4951–4968.
- Le Roy, E., Sanial, V., Lacan, F., van Beek, P., Souhaut, M., Charette, M. A., & Henderson, P. B. (2019). Insight into the measurement of dissolved <sup>227</sup>Ac in seawater using radium delayed coincidence counter. *Marine Chemistry*, *212*, 64–73.
- Shaw, T. J., & Moore, W. S. (2002). Analysis of Ac-227 in seawater by delayed coincidence counting. *Marine Chemistry*, *78*(4), 197–203.